

MULTIDIMENSIONAL VISCOELASTIC MODELING OF SILICON OXIDATION
AND TITANIUM SILICIDATION

By

STEPHEN CEA

A DISSERTATION PRESENTED TO THE GRADUATE SCHOOL
OF THE UNIVERSITY OF FLORIDA IN PARTIAL FULFILLMENT
OF THE REQUIREMENTS FOR THE DEGREE OF
DOCTOR OF PHILOSOPHY

UNIVERSITY OF FLORIDA

1996

Copyright 1996

by

Stephen Cea

ACKNOWLEDGMENTS

First I would like to thank my advisor Dr. Mark E. Law for all his guidance, support and all he has taught me throughout my stay here. I would also like to thank Drs. Jerry G. Fossum, Robert M. Fox, Kevin S. Jones and Sheng S. Li for their support as members of my doctoral supervisory committee.

I would also like to thank the many people who have helped during my graduate career. I would like to thank Jim Slinkman of IBM and the AFM crew for all their help with my experimental samples. I would also like to thank Dr. Mark Tran and Dr. Martin Giles of Intel and Dr. Stephen Pearton of UF for annealing various samples for me. I would also like to thank the various people at Stanford University who helped me during my stay there, including Dr. Mike Deal, Dr. Peter Griffin, Peter Smeys and Robin King. I would like to thank Brad Herner for all his sample prep help and advise. I would also like to thank Scott Luning and Roger Alvis of AMD for their mentoring and friendship; I will always remember the days of Five O. I would like to thank Mary Turner for keeping me in line. I would also like to acknowledge the support of the Semiconductor Research Corporation.

My stay in Gainesville has been very rewarding because of the many friends I have made while here. I will always remember the "happy hour" crew of Keith Green, Doug Weiser,

Hernan Rueda, Dave Zweidinger, Samir Chaudhry, Srinath Krishnan, Jonathan Brodsky, Ming-Yeh Chuang and Chih-Chuan Lin to name a few. I would also like to thank the roommates I have had during my stay in Gainesville, including Ed Cometz, Marty Weiss and Jon Brodsky. I would also like to thank the "-boys" Steve Reitberg, Al Delzell and Cory Gill.

Lastly, I would like to thanks my family especially my parents Mike and Doris Cea, my brother Anthony Cea and my grandmother Frances Boelke. Their support and love have always been there for me. I would also like to acknowledge the love and support of my girlfriend Janet Wall; she always keeps a smile in my heart.

TABLE OF CONTENTS

ACKNOWLEDGMENTS	iii
ABSTRACT	vii
CHAPTERS	
1. INTRODUCTION	1
1.1 LOCOS and Modified LOCOS	2
1.2 Silicides in VLSI Processes	5
1.3 Summary	6
2. MODELS FOR MATERIAL GROWTH	8
2.1 Introduction to Modeling Growth Processes	8
2.1.1 Diffusion and Reaction	9
2.1.2 Stress Due to Thin Films	13
2.1.3 Material Models in FLOOPS	19
2.2 Oxide	20
2.2.1 Deal Grove Model for Oxidation of Silicon	20
2.2.2 Volume Expansion and the Flow Solution	22
2.2.3 Stress Effects on Growth	26
2.2.4 Mechanical Models used for the Materials used in LOCOS	27
2.3 Silicide	32
2.3.1 Reaction Kinetics	33
2.3.2 Change of Volume and Stress due to Silicide Growth	35
2.3.3 Silicide Materials Models	38
2.4 Summary	40
3. MODEL IMPLEMENTATION	42
3.1 Numerics	42
3.1.1 FEM	44
3.1.2 Stress Interpolation	64
3.1.3 Nonlinear and Stress dependencies	65
3.1.4 Implementation of Newton's Method	69
3.2 Object-Oriented Techniques	72
3.2.1 Silicide/Oxide Physics	73
3.2.2 FEM Numerics	75
3.3 Summary	76
4. ONE DIMENSIONAL SILICIDE SIMULATIONS AND EXPERIMENTS ...	77
4.1 Simulation of Titanium Silicide Reaction Kinetics ...	77
4.1.1 Furnace Annealing of Titanium and Silicon	78
4.1.2 Furnace Annealing of Titanium and Amorphous Silicon	83
4.1.3 Rapid Thermal Annealing of Titanium and Silicon	87
4.2 Experiments in the RTA Growth of Titanium Disilicide	89

4.2.1 Overview of Experiment	91
4.2.2 Experimental Modeling	93
4.3 Summary	96
5. TWO DIMENSIONAL SILICIDE GROWTH EXPERIMENTS AND SIMULATIONS	99
5.1 Two-Dimensional Salicide Simulations	99
5.2 Two-Dimensional Experiments	104
5.2.1 Experimental Design	105
5.2.2 Experimental Results	106
5.3 Stress Dependent Silicide Simulations	112
5.3.1 Simulation of Two Dimensional Experiments	112
5.3.2 Salicide Simulations	115
5.4 Summary	121
6. THREE DIMENSIONAL OXIDATION SIMULATIONS	122
6.1 Calibration of Oxide Models	124
6.1.1 Experimental Details and Results	124
6.1.2 Calibration Procedure	125
6.2 Calibration of Nitride Models	131
6.3 Three Dimensional Simulations	134
6.4 Summary	138
7. SUMMARY AND FUTURE WORK	140
REFERENCES	145
BIOGRAPHICAL SKETCH	150

Abstract of Dissertation Presented to the Graduate School
of the University of Florida in Partial Fulfillment of the
Requirements for the Degree of Doctor of Philosophy

MULTIDIMENSIONAL VISCOELASTIC MODELING OF SILICON OXIDATION
AND TITANIUM SILICIDATION

By

Stephen Cea

December, 1996

Chairman: Dr. Mark E. Law

Major Department: Electrical and Computer Engineering

Semiconductor process simulation is used to help develop new process technologies and to improve existing processes. This work consists of the development and implementation of physically based models for the multidimensional simulation of silicon oxidation and titanium silicidation.

The model used to simulate both of these processes has two steps. First, solve for the diffusion and reaction of the reactant. Second, solve for the deformation caused by the volume change that accompanies the reaction. The deformation is solved for using a stress dependent viscoelastic model. The stress caused by the volume changes can influence the growth of either titanium silicide or silicon dioxide.

The growth models were implemented using the finite element method in an object-oriented environment. Newton's method is used to solve for the nonlinear stress dependent growth. The use of object oriented techniques has speeded model development and allowed code sharing between the two growth systems.

One- and two-dimensional silicide growth experiments have been performed to calibrate the models for titanium silicide growth. The growth exhibits diffusion limited behavior for a wide range of experimental conditions. Silicide growth on trenches is used to determine that silicide growth is affected by mechanical stress. High compressive stress reduces the diffusion of silicon through the growing silicide film.

Three-dimensional oxidation simulations are compared to oxidation experiments on nitride fingers. The amount of nitride lifting is increased as the width of the nitride line decreases. This trend is seen in the simulations which match the experiments well.

CHAPTER 1 INTRODUCTION

As semiconductor processing increases in complexity, process simulation has become more important. Process simulation is used to shorten the development cycle of new processes and to improve existing processes. Two important process steps to be simulated in modern silicon processing are oxidation and silicidation. The stresses that arise from these steps must also be accurately simulated in the growing layers and in the silicon substrate. This dissertation will discuss the oxidation and silicidation models developed in the process simulator FLOOPS (Florida Object Oriented Processing Simulator).

The oxidation of silicon is used to grow gate oxides and field oxides. Field oxides are grown as part of the isolation process. There are two main types of isolation used today: trench isolation or some form of LOCOS (LOCAl Oxidation of Silicon). LOCOS is discussed in the next section. Silicidation, which is used to contact the drain, sources and gates in MOS semiconductors and as a local interconnect material, will be discussed in section 2.

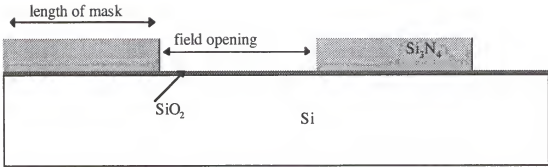


Figure 1-1: LOCOS structure before growing field oxide.

1.1 LOCOS and Modified LOCOS

In silicon processing one of the most important steps is the device isolation. The majority of technologies used today use LOCOS or modified LOCOS isolation techniques. The first step is to grow a pad oxide and then deposit silicon nitride. The nitride is patterned to expose the field areas. Figure 1-1 shows a LOCOS process at this step. The exposed areas are oxidized to grow the desired thickness of isolation oxide. Figure 1-2 shows the grown LOCOS structure. The final step is to strip the nitride.

Conventional LOCOS suffers from several drawbacks for submicron technologies. As the width of the field region decreases, the thickness of the field oxide decreases in comparison to wide mask openings[1]. There is a large bird's beak encroachment into the active area. Nonplanar topologies

are produced, which makes lithography difficult. Pad ox punchthrough effects for narrow nitride lines are also seen[2]. Pad ox punchthrough occurs when the width of the nitride line mask is too narrow to prevent the pad ox from growing under the mask. This is obviously undesirable because now the device areas are not isolated from each other. As device dimensions shrink these effects are no longer just two-dimensional in nature, they are three-dimensional. The active area in submicron devices is so small and the devices so tightly packed together that three-dimensional simulations are needed to determine when these undesirable effects occur.

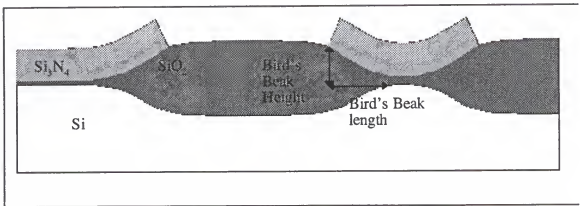


Figure 1-2: LOCOS structure after field oxidation.

In an effort to extend LOCOS type technologies into the submicron and deep submicron technologies, several modifications to the conventional LOCOS have been attempted. Some of the more successful strategies are FUROX (Fully-Recessed OXide), Poly Buffered LOCOS (PBL), and Sealed-

Interface Local Oxidation (SILO). The FUROX process involves recessing the silicon substrate so that the resulting profile is more planar. PBL involves modifying the mask stack to include a layer of polysilicon between the nitride and pad oxide. This tends to decrease the stress in the silicon by providing a pad layer between the padox and the nitride layer. Diffusion under the mask area decreases. The SILO process has a thin layer of nitride directly on the substrate followed by a layer of SiO_2 and another layer of Si_3N_4 . The layer of nitride on the Si reduces the lateral diffusion of oxide under the nitride. This results in a small bird's beak which can cause defects in the silicon due to the large stresses the SILO process can cause. As you can see these processes are similar to LOCOS isolations with some added steps to reduce the drawbacks of LOCOS.

From a modeling point of view, being able to accurately simulate conventional LOCOS is important. The increased understanding of the problems with LOCOS can help design modified LOCOS processes to alleviate these problems. Simulation can also help in determining if a modified process will work and what other problems it can introduce. The processes described above, as well as other modified LOCOS strategies, present new simulation challenges in terms of boundary conditions and materials for the simulation of isolation processes. In the sections to follow the oxidation models in the process simulator FLOOPS will be discussed.

1.2 Silicides in VLSI Processes

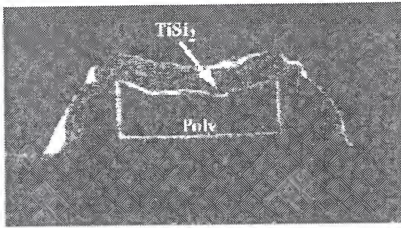
As device dimensions have decreased, both junction depths and gate lengths have decreased. This scaling has led to unacceptably high levels of sheet resistance. The most popular technique to overcome this problem is to use a Self-Aligned silicide (salicide) process. The silicide shunts the sheet resistance of the doped silicon, lowering the resistivity of those areas. In a typical titanium salicide process the first step is to form the spacer next to the gate. This is done with an isotropic deposition and anisotropic etch. The next step is the titanium deposition. Then an anneal at 650 °C in a nitrogen ambient is performed. This anneal forms the C49 phase of TiSi_2 , where the titanium was in contact with silicon and TiN on the exposed Ti surface. The TiN and unreacted Ti is stripped. A second anneal is performed to transform the phase of the TiSi_2 from C49 to the low resistivity C54 phase. It is well known that there are strange shapes formed during the salicide process. Bowing of the silicides on poly lines (Figure 1-3 a)[3] and narrowing of the formed silicide next to the spacer (Figure 1-3 b)[4] is commonly seen. Silicides are also used to replace polysilicon as a local interconnect. This greatly reduces the RC delay in silicon devices. It is important to be able to simulate these processes so that we can accurately determine the stresses in the films, the silicide shapes, and

the stresses in the substrate due to silicide growth as well as any stress or silicide growth effect on dopant diffusion.

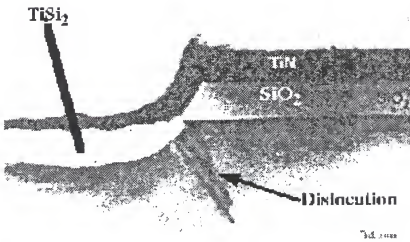
Most metals form silicides when reacted with silicon. There are two main categories of silicides used in silicon device processing: refractory metal silicides and near-noble metal silicides. Silicides are attractive for silicon processing due to their low resistivity and the stability of their contacts to silicon. To be useful for most device technologies, silicides must not react with SiO_2 , have low silicon consumption, and be stable at high temperatures. The silicides that best meet these requirements are the C54 phase of TiSi_2 and CoSi_2 . The silicide we have focused our research on is TiSi_2 because it is the most utilized in industry today. Due to the object oriented nature of FLOOPS, supporting additional silicides is not difficult.

1.3 Summary

Chapter 2 will describe the general models used to simulate growth process and then apply these models to both oxide and silicide growth. The third chapter will discuss the numerics and other software techniques used in programming these models into FLOOPS. Chapter 4 and 5 will describe simulations and experiments in TiSi_2 growth in one and two dimensions respectively. Chapter 6 will describe the calibration of the oxide growth code and apply the calibrated coefficients to three-dimensional simulations.



a)



b)

Figure 1-3: Silicide structures a) showing bowing of poly lines and b) narrowing next to spacer edge.

CHAPTER 2 MODELS FOR MATERIAL GROWTH

2.1 Introduction to Modeling Growth Processes

Modeling reactive diffusive growth processes consists of performing two steps that are repeated at each time step of the simulation. First, solve for the diffusion and reaction of the reactant through the growing layer. Second, account for the volume changes caused by the growth and solve for the stress caused by these volume changes in the surrounding layers. The grid is then updated and the next time step is solved. These two steps could depend on each other. For example the stress caused by the flow could affect the diffusion of the reactant as in oxide growth. This section will begin by looking at a general reaction and diffusion system. Several material models for solving for the stress in the system are discussed, as well as the models implemented in FLOOPS. In the final two sections the specifics of how each of these two steps are modeled in FLOOPS for the growth of SiO_2 and the silicidation of titanium in a nitrogen ambient will be shown.

2.1.1 Diffusion and Reaction

The formation of both SiO_2 and TiSi_2 are modeled using a Deal Grove like diffusion and reaction model. In this model, shown in Figure 2.1 a, reactant diffuses through the growing layer (AB) from the source of reactant (A) to the reacting interface(AB/B). At the reacting interface the molecules react to form the new material. There are three fluxes associated with this model: 1) the flux of reactant from the source to the interface between the source and growing layer, F_1 ; 2) the flux of the reactant as it diffuses through the growing layer, F_2 ; 3) the flux of the reacting species as it is consumed by the reaction to form the new layer of the growing material. In the steady state condition, the three fluxes will be equal and any one of them could be the rate limiting step.

These fluxes are shown in Figure 2.1b. F_1 is defined as

$$F_1 = k_i(C^* - C_s) \quad (2.1)$$

where C^* is the equilibrium concentration of reactant at the A/AB interface, C_s is the reactant concentration across the interface and k_i is the transfer coefficient across the interface. If k_i is large, C_s will be equal to C^* and this flux will not be a rate limiting step. The flux of atoms across the growing layer F_2 is given by

$$F_2 = -D \frac{(C_s - C_r)}{x_g} \quad (2.2)$$

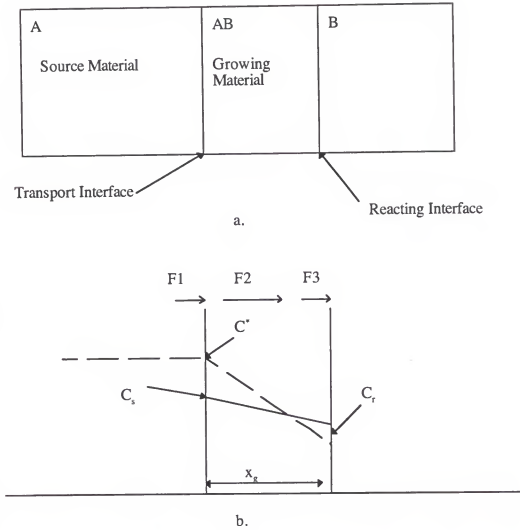


Figure 2-1: A general model of Reactive diffusive a) the materials b) the concentration across the growing material.

where D is the diffusion coefficient of the reactant in the growing layer, C_r is the reactant concentration at the reacting interface and x_g is the thickness of the growing layer. The flux at the reacting interface is

$$F_3 = k_s C_r \quad (2.3)$$

where k_s is the reaction rate coefficient. In steady state the three fluxes can be set equal and the unknowns C_s and C_r are given by

$$C_s = \frac{C^* \left(1 + \frac{k_s x_g}{D} \right)}{1 + \frac{k_s}{k_t} + \frac{k_s x_g}{D}} \quad (2.4)$$

$$C_r = \frac{C^*}{1 + \frac{k_s}{k_t} + \frac{k_s x_g}{D}} \quad (2.5)$$

The growth rate dx_g/dt can now be calculated by using equations 2.4 and 2.5 in equation 2.3 and defining N_1 as the number of molecules of reactant incorporated into a unit volume of growing material. The growth rate is

$$N_1 \frac{dx_g}{dt} = F_3 = \frac{k_s C^*}{1 + \frac{k_s}{k_t} + \frac{k_s x_g}{D}} \quad (2.6)$$

Equation 2.6 can be solved by applying an initial boundary condition that $x_g = x_i$ at $t=0$. The solution is

$$\frac{x_g^2}{B} + \frac{x_g}{B/A} = (t + \tau) \quad (2.7)$$

where

$$B = \frac{2DC^*}{N_i} \quad (2.8)$$

$$\frac{B}{A} = \frac{k_{eff}C^*}{N_i} \quad (2.9)$$

$$k_{eff} = \frac{k_s k_i}{k_s + k_i} \quad (2.10)$$

$$\tau = \frac{x_i^2 + Ax_i}{B} \quad (2.11)$$

B is called the parabolic rate constant, B/A is the linear rate coefficient and τ represents the time needed to account for the initial thickness at $t=0$. For a specific growth process the parameters B and B/A are usually fit to experiment. From these diffusivities, reaction rates and transfer coefficients are extracted. The specifics of how this reactive-diffusive model is applied to oxidation and silicidation will be discussed in the sections 2.2.1 and 2.3.1.

2.1.2 Stress Due to Thin Films

After the reaction takes place there is a volume change in the materials involved in the growth. This volume change can cause deformation and/or stress in the materials involved in the reaction as well as any surrounding materials (including the substrate). These stresses can influence the growth rate, cause defects in the silicon substrate or create voids in polycrystalline films. It is very important to account for the stress caused by film growth and other sources, for example, thermal mismatch. This section will discuss stress and some models that can be used to solve for the stress in growing and surrounding materials.

Stress in thin films can be divided into two categories intrinsic and extrinsic. Extrinsic stresses are caused by the differences between thermal expansion coefficients of the thin film and the substrate as the wafer is subjected to thermal cycling[5]. There are many sources of intrinsic stress. Intrinsic stresses can be caused by the volume change caused by the growth of thin films like oxides and silicides. It also arises from precipitation, annihilation of defects, phase transformation, grain growth and structural changes. The main focus of this work is to look at intrinsic stresses due to volume changes and their effects on growth. Thermal stresses and other intrinsic stresses will also be briefly addressed and their inclusion discussed.

An equation that describes a property of a material is called a constitutive relationship. One type of constitutive relationship relates stress to strain or strain rate because it describes the mechanical properties of a material. There are many mechanical models available. The following sections will discuss several simple constitutive relationships: an elastic model, a viscous model and a maxwellian viscoelastic model. Figure 2.2 shows the typical mechanical elements associated with these models. Stress dependent viscosity in the viscous and viscoelastic models will also be examined. The ability of the models available in FLOOPS to model the majority of the material behaviors needed, as well as most of the sources of stress in thin films, will be demonstrated.

2.1.2.1 Linear elastic

Most solid materials display a memory affect when they are deformed. When a force is applied to these materials they deform relative to their initial configurations and when the force is removed they return to that initial state. This type of material is known as a Hookean elastic solid. These materials obey Hooke's law which states that a stress tensor is linearly proportional to the strain tensor. One simple example of this type of behavior is a linear spring shown in Figure 2-2a. Linear elastic behavior for an isotropic material, assuming no initial stress, is given by

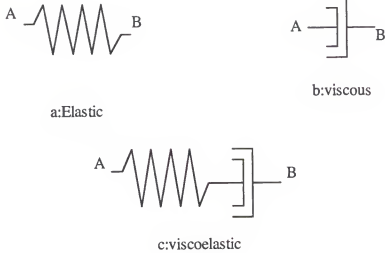


Figure 2-2: Typical mechanical elements for the common material models.

$$\sigma = D\varepsilon \quad (2.12)$$

where σ is the stress tensor, ε is the strain tensor, and D is a tensor of elastic constants. The elastic constants are functions of the Young's Modulus and Poisson's ratio of the materials. To demonstrate Young's modulus and Poisson's ratio consider Figure 2-3, which shows a plate of length l , width W and thickness T (into the page). The thin film is being stretched by a force F applied to the area of $W \cdot T$. This increases the length of the film by Δl . The stress for this specimen can be written as $\sigma = Y\varepsilon$, where Y is the Young's modulus, the stress is F/A and the strain is $\Delta l/l$. Poisson's ratio is expressed as $\frac{\Delta T}{T} = \frac{\Delta W}{W} = -\nu \frac{\Delta l}{l}$, where ν is the

Poisson's ratio. The Poisson's ratio is usually a positive number less than 0.5. A material with a Poisson's ratio of 0.5 is incompressible. This means that the volume doesn't change even though the shape does. For the simple one dimensional case, like the spring in Figure 2-2a, D is equal to the Young's modulus of the material. While most solids behave as Hookean elastic solids over some range of temperatures, stresses, and strains, most have a more complex behavior at high temperatures, stresses, and strains.

2.1.2.2 Linear viscous

Linear viscous materials have no memory effect. When forces are applied to these materials they flow or deform in response to the force as long as it is applied. This type of behavior is typified by the dashpot in Figure 2-2b. If point B is fixed and a force is applied to point A then the dashpot will deform in response to the force. When the force is

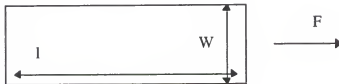


Figure 2-3: Thin film of dimensions $l \times W \times T$ being stretched by a force F .

removed then point A will remain at the position it was in when the force was removed. In linear viscous materials the stress is linearly proportional to the strain rate and can be expressed as

$$\sigma = D\dot{\epsilon} \quad (2.13)$$

where D now represents the tensor of viscosities for the material. For a simple one dimensional viscous element $D=2\mu$, where μ is the viscosity. Viscous materials can be incompressible which means that the material's volume can't change even though its shape does. Fluids are the materials that most often exhibit viscous behavior.

2.1.2.3 Linear viscoelastic

The behavior of viscoelastic materials lie between viscous and elastic. A Maxwell viscoelastic material is represented by the mechanical model shown in Figure 2-2c. It consists of a viscous and an elastic element in series. This model can exhibit either viscous or elastic behavior depending on the time scale of the observation in relation to the relaxation time of the element. If, in Figure 2-2c, point B is fixed and a force is applied at point A all the movement will be in the spring initially. Over time the spring will relax to it's original length and the displacement will be transferred to the dashpot. The behavior of the element is given by

$$\frac{\dot{\sigma}}{G} + \frac{\sigma}{\mu} = \dot{\epsilon} \quad (2.14)$$

whose solution for constant growth rate and viscosity is

$$\sigma = \mu \dot{\epsilon} \left(1 - e^{-\frac{t}{\tau}} \right) \quad (2.15)$$

Where μ is the viscosity, t is the time and τ is the relaxation time for a linear maxwellian viscoelastic material

$$\tau = \mu / G. \quad (2.16)$$

Here G is the shear modulus which is represented by

$$G = \frac{Y}{2(1+\nu)} \quad (2.17)$$

where Y and ν are the Young's modulus and Poisson's ratio of the material.

2.1.2.4 Nonlinear flow

At high strain rates most materials display nonlinear or plastic flow characteristics. One of the most common nonlinear flow models is the hyperbolic sine or Eyring model. This model has been applied to oxide growth with great

success by Rafferty[6]. In this model the viscosity is stress dependent and given by

$$\mu = \mu_0 \frac{\sigma_s / \sigma_c}{\sinh(\sigma_s / \sigma_c)} \quad (2.18)$$

where μ_0 is the low stress viscosity, σ_c is the stress above which the material softens and σ_s is the maximum shear stress. This type of nonlinear viscosity can be used for the viscous flow of section 2.1.2.2 or the viscoelastic flow of section 2.1.2.3.

2.1.3 Material Models in FLOOPS

In FLOOPS the most used material model available is the viscoelastic model. Nonlinear or stress dependent viscosity given by equation 2.18 is available in the model. This material can exhibit either elastic or viscous behavior depending on the time frame of interest in relation to the relaxation time. For times much less than τ the behavior will be elastic and for times much longer than τ the behavior will be viscous. This general response makes this model ideal for process simulation where a wide range of material responses, temperatures, and times need to be simulated. Elastic behavior is simulated by using a large viscosity in the viscoelastic model, thereby giving the material a large relaxation time. This has worked well for a number of

elastic problems including the stress due to nitride stripes where both the nitride and silicon are elastic materials.

2.2 Oxide

In this section the specifics of how the models from section 2.1 have been applied to the modeling of oxidation will be discussed. Previous models for the thermal oxidation of silicon will be discussed and compared to this work. The main difference between oxidation simulators are the mechanical material models used for the oxide, nitride and polysilicon films, stress effects on growth and how the models are discretized and solved. All physically based simulation efforts use the Deal Grove models for solving for the diffusion and reaction of oxidant. The choice of material models to use in the simulation of oxidation flow has been a very active research topic.

2.2.1 Deal Grove Model for Oxidation of Silicon

The general model of reaction diffusion shown in Figure 2.1 and developed in section 2.1.1 is applied to the oxidation of silicon shown in Figure 2-4. The reactant for this system is an oxidant, H_2O for wet oxides and O_2 for dry oxides. The source of oxidant is the gas, the growing material is SiO_2 and the reacting interface is the Si/SiO_2 interface. The first flux, the transport of oxidant across

the gas/SiO₂ interface is readily achieved so it is not the rate limiting step. In other words $C_s = C^*$ and $k_{eff} = k_s$. In eq. 2.7 B/A is now given by

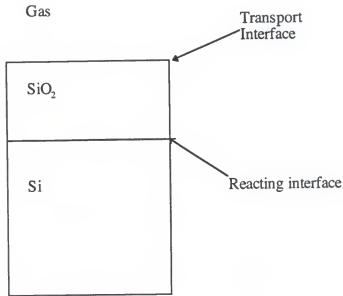


Figure 2-4: Application of the general model in Figure 2.1a to silicon oxidation.

$$\frac{B}{A} = \frac{k_s C^*}{N_l} \quad (2.19)$$

and B is the same as equation 2.8. Of course eq. 2.7 is now the well known Deal Grove model of oxide growth[7]. The linear and parabolic coefficients for oxidation in both dry and wet ambients has been exhaustively studied and are summarized by Rafferty[6]. Table 2-1 shows the default coefficients used in FLOOPS for oxidation growth on <100> Si.

In LOCOS technologies the diffusion of oxidant is

usually masked by Si_3N_4 . Figure 2-5 shows the diffusion model for oxidant diffusion and reaction complete with boundary conditions. In Figure 2-5 the oxidant is available at the gas/ SiO_2 interface at a concentration of C^* . This is because k_t in eq. 2.1 is large. The oxidant diffuses through the growing oxide according to Fick's law in steady state. The reaction at the Si/SiO_2 interface is due to the balance of the reactive diffusive fluxes. The flux into the nitride is zero.

Table 2-1: Oxidant diffusion coefficients used in FLOOPS

Ambient	B_o um ² /min	E_B eV	B_o/A_o um/min	$E_{B/A}$ eV
Dry	12.867	1.23	1.038e5	2.0
Wet	7.0	0.78	2.95e6	2.05

2.2.2 Volume Expansion and the Flow Solution

After the solution of the oxidant diffusion and reaction, the concentration of oxidant at the Si interface is used to determine the amount of oxide formed. The formation of silicon dioxide at the Si/SiO_2 interface is accompanied by a volume expansion. The molar volume of Si in SiO_2 is larger than in Si, which causes a net expansion at the oxide/silicon interface. This expansion causes stress in

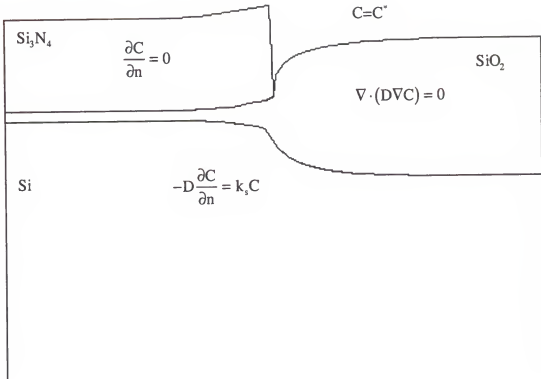
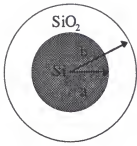
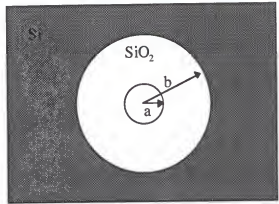


Figure 2-5: Diffusion and reaction of oxidant during thermal oxidation.

LOCOS structures and the oxidation of nonplanar structures like trenches or cylinders. Cylinders are an interesting structure to investigate for two reasons: first it is easy to explain the stress that arises and second they are the structures that have been used to experimentally determine the stress effects on oxidation. Kao[8] oxidized cylinders of varying radii in both dry and wet ambients at temperatures ranging from 800 - 1200 °C on both convex and concave surfaces. The thickness of oxide grown decreased with decreasing radius (which produces increased stresses in the oxides). Figure 2-6 shows schematics for convex and concave structures.



a.



b.

Figure 2-6: Types of structures used by Kao for a)convex and b)concave surfaces.

The convex structure or cylinder produces tensile pressure in the oxide. This is due to the fact that as the oxide is lifted away from the Si/SiO₂ interface it needs to fill a larger area and so it has to stretch. Similarly, for the concave structures or holes the pressure is compressive because the new oxide is forced to fill a volume that is smaller than its original volume. Both holes and cylinders produce a compressive normal stress. The results of this experiment will be further discussed in section 2.2.4 when the stress effects of growth are presented.

The growth of LOCOS structures also produces stresses in the growing oxide, the surrounding thin films, and the silicon substrate. The origin of this stress is mainly from any oxide formed under the nitride mask that expands against the nitride. This produces stresses in the oxide layer and

the bending of the nitride causes it to be stressed. Figure 2-7 shows the simulated contour plots of the stresses generated during the oxidation of a LOCOS structure at 1000 °C for 30 min. There is a large compressive pressure under the nitride due to the volume expansion associated with oxide growth. The bending of the nitride causes compressive

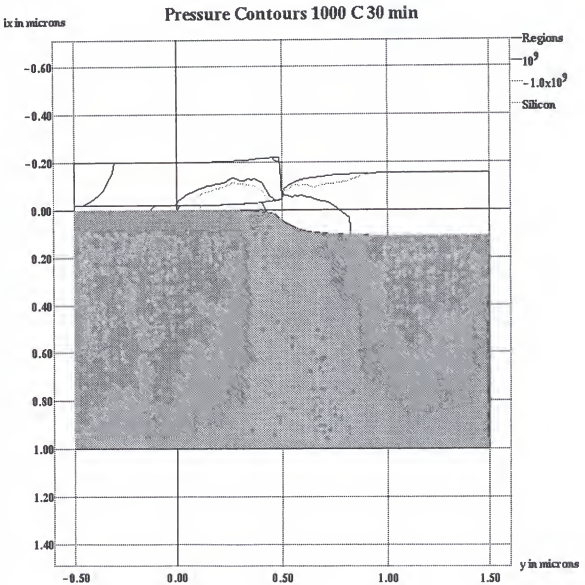


Figure 2-7: Pressure contours (+ compression) in a LOCOS structure

pressure on the top section of the nitride and tensile pressure along the bottom of the nitride, which is being stretched.

2.2.3 Stress Effects on Growth

The stress generated by thermal oxidation is known to reduce both the reaction rate, k_s in equation 2.19, and the diffusivity, D in equation 2.8. This was reviewed extensively by Rafferty[6]. In this section we will give a brief review of how the stress affects k_s and D .

A compressive stress normal to the Si/SiO₂ interface will reduce the reaction rate k_s by

$$k_s = k_{s0} e^{-\sigma_{nn} V_r / kT} \quad (2.20)$$

where k_{s0} is the reaction rate from the Deal Grove model, σ_{nn} is the stress normal to the Si/SiO₂ interface and V_r/kT is the activation volume divided by Boltzmann's constant and the temperature in °K. The derivation of this expression was first done by Kao.[9] The diffusivity is influenced by pressure. The diffusivity as a function of pressure is given as

$$D = D_0 e^{-PV_r / kT} \quad P > 0 \quad (2.21)$$

and either $D=D_0$ for $P<0$ or

$$D = \min(D_{\max}, D_{\text{enh}}) \quad P < 0 \quad (2.22)$$

where D_0 is the diffusivity from the Deal Grove formulation, P is the hydrostatic pressure, D_{\max} is the maximum diffusivity, D_{enh} is the D from eq. 2.19 with $P<0$ and V_d/kT is again the activation volume divided by Boltzmann's constant and the temperature in $^{\circ}\text{K}$. The term D_{\max} is used to clamp the increase in diffusivity due to tensile pressure. In Rafferty's original fit to Kao's data, he didn't allow D to increase with tensile pressure because the data couldn't be fit over the range of cylinder radii for wet oxides. To further confuse things equation 2.20 is supported in SUPREM IV[10] which Rafferty developed as part of his PhD work. Sutardja and Oldman[11] have used equation 2.20 and obtained fits to Kao's data. In this study D_{\max}/D_0 ranged from 1.0 at 1200 $^{\circ}\text{C}$ to 2.0 at 800 $^{\circ}\text{C}$. Kao's data on dry oxidation shows an increase for convex cylinders of large radius which would tend to indicate that D increases with tensile pressure.

2.2.4 Mechanical Models Used for the Materials Used in LOCOS

All of the recent simulation programs for oxidation modeling include stress effects on the growth, but they differ in the material models for the three main materials used today in modern LOCOS processes. The three materials

are oxide, nitride and polysilicon. The first numerical modeling of oxide growth was by Chin et al.[12]. Chin modeled oxide as an incompressible viscous fluid and nitride as an elastic beam. Maxwell's linear viscoelasticity was used to model both the oxide and nitride by Matsumoto and Fukuma[13]. Poncet[14] used a linear elastic model for the oxide and nitride materials. In this work, he also details an elasto-visco-plastic model and introduces stress effects in the diffusion equations. The details of the stress dependencies are not evident but they are mentioned. All of these early works showed promise as well as the ability to accurately simulate some structures. Due to the lack of data on the materials and reactions, these efforts were not well calibrated so evaluating them is difficult.

After the important experimental work of Kao[8], there was ample data to begin calibrating the simulators that were developed. Umimoto et al.[15] extended the work of Chin[12] to include the original stress dependencies proposed by Kao[8]. In Kao's original model the viscosity was

$$\mu = \mu_0 \exp(\alpha p), \quad \alpha \geq 0. \quad (2.23)$$

where p is the pressure. The main flaw in this model is that the viscosity increases with pressure. This makes modeling concave structures impossible because there is a positive feedback loop present, the compressive stress increases the viscosity which increases the compressive pressure. In

Uemimoto's work equation 2.21 is used only for tensile pressures. This simulator seems to be able to model a number of LOCOS cases in two and three dimensions[16] but it can't model the oxidation of concave structures which is the basis for calibrating stress dependent oxidation.

In the late 1980's the CREEP[11] and SUPREM IV[6,10] oxidation simulators were released. Their models are very similar and feature stress dependent diffusivity, reaction rates, and viscosity. Both modeled the oxide as a nonlinear viscous incompressible material. CREEP treated Si_3N_4 as linear elastic. SUPREM IV uses a linear viscous incompressible model for Si_3N_4 .

An experiment by Rafferty and Griffin was used as evidence that a viscous incompressible model should be used for the nitride mask[17]. The experiment consisted of growing a LOCOS structure, then annealing some of structures in an inert ambient for long times at the growth temperatures. The structures, with and without the additional anneal, were nearly identical. This showed that the nitride was not elastic because if it was, the nitride would have relaxed to its original position, because the viscous oxide would flow in response to the force from the nitride. This model was used in SUPREM IV. The grown structures were modeled and the viscosity for the nitride was extracted. Simulations run using FLOOPS using a viscous model for the oxide and elastic model for nitride confirm

that the nitride would return to its original position. On the other hand simulations using nonlinear viscoelastic models for the nitride and oxide showed no movement during the further anneal. Obviously this experiment can't be used as proof of the validity of either model.

More recent simulators, namely NOVEL[18] and IMPACT 4[19], have used a nonlinear viscoelastic model for the oxide. There has been much debate on the correct model or sufficient model for SiO_2 . The difficulty arises because oxide displays elastic behavior at low temperatures and viscous flow at very high temperatures ($>1400^\circ \text{C}$). Unfortunately the growth of oxide in silicon processing is done at intermediate temperatures, $800^\circ\text{--}1100^\circ \text{C}$. The viscoelastic model is definitely more applicable for modeling oxide growth through the whole range of temperatures. Many reports[6,20,21] have plotted stress as a function of thickness of oxide grown on a cylinder using both the nonlinear viscoelastic and nonlinear viscous models. The plots for the stress from nonlinear viscoelastic and nonlinear viscous models eventually converge at a certain oxide thickness. For example at 1000°C the thickness is approximately 500 Angstroms. This has led many to assume that a viscous model is sufficient for modeling oxide growth at high temperatures. The fact that is overlooked by many is that these solutions, as pointed out by Hu[21], are for the oxide at the outer surface of the oxide. These volumes of oxide were the first to be formed and have therefore been

there since the start of the oxide growth. New volumes of SiO_2 are constantly generated during the oxidation of silicon which would have zero elapsed time. So throughout the oxide film there will be volumes of oxidant that will have as their elapsed time anywhere from zero to the total oxide growth time. One of the important things to realize is that the stress at the Si/SiO_2 interface will be least accurate, due to ignoring elastic effects. This is also where it is needed to be most accurate because of the stress effect on k_s . Viscoelasticity is also important because it allows for the addition of thermal stresses and keeps track of the stress from process step to process step. The recommended oxide model in FLOOPS is nonlinear viscoelastic. Nonlinear viscoelastic behavior has been applied to nitride behavior successfully by Senez[19] and a similar model is used in FLOOPS. This model uses a nonlinear viscoelastic element for the deviatoric or shear component of the stress tensor and an elastic element for the pressure or dilatational component of the stress.

The correct material model to use for polysilicon is still under study. Commercial versions of SUPREM use a viscous model, while Senez has used an elastic model. Recent experimental results by Nagel et al[22] show that the stress in pbl causes voids in the polysilicon and that the poly seems to flow. This is clearly not the behavior of a simple elastic material. Polysilicon is almost certainly viscoelastic and possibly includes a stress dependent

viscosity. More investigation is needed to see if the Eyring model will be applicable. The determination of all the material parameters like Young's Modulus, Poisson's ratio and viscosity will have to be determined. They are almost definitely not the same as crystalline silicon and will probably vary with grain size.

2.3 Silicide

The modeling and understanding of silicide growth is nowhere near as mature as for oxidation. This section will apply the models discussed in section 2.1 to the modeling of titanium silicidation. Titanium silicide growth can be performed using furnace annealing or rapid thermal annealing (RTA) techniques. The most common technique is an RTA in a nitrogen ambient. This produces the growth of TiN as well as TiSi_2 . The diffusion/reaction system of section 2.1.1 will be used to model the growth of titanium silicide and nitride. The first part of this section will discuss the reaction kinetics of these reactions. The mechanical models for all the materials in a typical silicide process will also be discussed. TiSi_2 has two phases, the metastable C49 and the low resistivity C54 phases. There are two anneals used in a silicide process. The first is usually between 600-700 °C. This anneal is used to grow the silicide and the phase formed at this stage is the C49 phase. The temperature of the first step must be kept below 700 C to prevent the titanium from

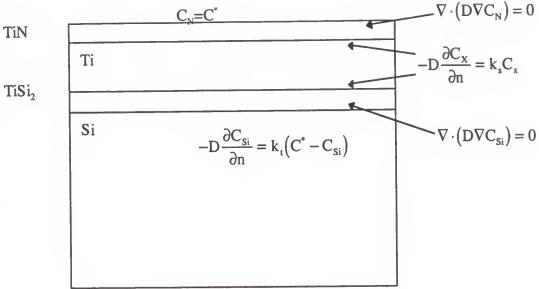


Figure 2-8: Silicide diffusion and reaction systems.

reacting with the spacer material, usually SiO₂. The second anneal is performed after stripping off the unreacted Ti and the formed TiN. The purpose of this anneal is to transform the silicide to its low resistance phase. This modeling work has dealt with trying to accurately model the shape of the silicide contacts so most of the work has been done modeling the first anneal step.

2.3.1 Reaction Kinetics

The typical reaction taking place during the silicide process are shown in Figure 2-8. Silicon diffuses through the growing silicide and reacts at the Ti/TiSi₂ interface. Nitrogen diffuses through the TiN layer to react at the Ti/TiN interface. In FLOOPS the growth of both TiN and TiSi₂

are modeled. Both reactions are modeled using eqs. 2.7 - 2.11. The growth of TiSi_2 has been found to be diffusion limited for both furnace annealing[23,24] and RTA[25,26]. The cleanliness of the Si surface before titanium deposition is very important and differences between surface preparation make comparing results from various studies hard. There are several trends that can be noticed. The reaction in a nitrogen ambient is slower than in argon. This is reportedly due to blocking of the grain boundaries by the nitrogen[27]. This is precisely the reason that the formation of TiSi_2 is done in a nitrogen ambient, because it prevents bridging of the spacers. This brings up an interesting point, that the D in equation 2.8 is the effective diffusivity of Si through the silicide and has components of grain boundary diffusion and bulk diffusion. The k_{eff} in equation 2.10 is probably more due to the mass transfer of silicon than the reaction at the TiSi_2/Ti interface. The amount of silicide grown on heavily doped substrates, both n and p, is less than on lightly doped substrates. Pico[24] found reaction limited growth on $\langle 111 \rangle$ Si. Increased doses of BF_3 implants were found to decrease the thickness of TiSi_2 formed by RTA.[28] This was attributed to increased native oxide growth on the heavily doped substrates. All of these signs point to the transport of Si changing, although it is possible that the dopants are forming compounds like TiAs [29] that block the grain boundaries and inhibit Si diffusion. Concoran et. al[30] have reported that grain boundary diffusion and grain

growth are dominant. These results are for anneals at 750 °C. At this temperature both C49 and C54 phases were present. This complicates the kinetic analysis because there are phase transitions taking place. This study does point out the importance of grain boundary diffusion but because it was performed at such a high temperature it is of limited use for the modeling of the typical two step silicide process.

There has been less work on the growth of TiN. Krooshot et. al[31] reported that 85% of a 150 nm Ti film and 74% of a 60 nm Ti film formed TiSi_2 , the remainder formed TiN. Jongste[32] reported that 20 nm of deposited Ti layers formed $\text{TiN}_x\text{O}_{1-x}$ and that 80% of the remaining Ti is transformed into titanium disilicide. In FLOOPS we have used values for TiN kinetics that reflect these results. The default coefficients for the growth of both TiSi_2 and TiN used in FLOOPS will vary depend on the ambient of the anneal, the deposition pressure of the titanium and the surface cleanliness. Several studies will be modeled in chapter 5 and fits for each one will be shown.

2.3.2 Change of Volume and Stress Due to Silicide Growth.

The solution of the diffusion of silicon is followed by the consumption of Si and Ti and the growth of TiSi_2 and solving for the flow of the surrounding materials. The boundary condition at the Si/ TiSi_2 interface is

$$v = \frac{k_t(C - C^*)}{N_i} \quad (2.23)$$

the Ti consumption at the TiSi_2/Ti interface is

$$v = \frac{\alpha_u k_s C}{N_i} \quad (2.24)$$

and the volume expansion at the TiSi_2/Ti interface is

$$v_{\text{tisi}} = \frac{\alpha_{\text{tisi}} k_s C}{N_i} \quad (2.25)$$

where C is the concentration of Si, N_i is as in equation 2.6, k_s is the reaction rate, k_t is the transfer coefficient, α_{tisi} is related to the expansion of the formed silicide, and the α_u is the consumption of the Ti.

The formation of TiSi_2 results in a net decrease in volume of 25%. The silicide film sinks into the substrate as it is formed. The origin of stress due to this reaction should be expected even in the one dimensional case. There have been various studies of the stress from the formation of TiSi_2 . Jongste et al. has performed several in-situ studies on the stress generated during the annealing of Ti Si multilayers.[33,34] In one RTA study three Si/Ti ratios in the multilayers was used: 1.9, 2.1 and 2.4. In this study C49 TiSi_2 was formed and the stress during and after the

formation was studied. As expected there was a tensile stress due to the 25% volume contraction after the formation of the TiSi_2 . After further annealing the stresses relaxed. The relaxation was greater at higher temperatures and for Si/Ti ratios > 2.0 . These results will be discussed more in section 2.3.3.

Chen et al. also performed in-situ stress measurements during the formation of TiSi_2 . [35] This study used deposited Ti films that were then annealed. In this case a compressive stress due to the growth of TiSi_2 is found. The stress is found to decrease abruptly at temperatures above 700 °C. The fact that a compressive stress is found is confusing because of the volume decrease during silicide growth. Although, if the volume from the silicon is not taken into account then the compressive stress makes sense. Also this doesn't take into account the complex behavior of the grains and grain boundary diffusion. Compressive stress has also been reported in other studies of thin Ti films on Si reaction [36]. In this study the C49 TiSi_2 showed stress relaxation at 667 °C but not at 550 °C. The development of intrinsic stresses due to growth is very complex so it is not surprising that a compressive stress is generated for these cases. This means the stress evolution during silicide formation is very complex and it's effect on growth may be difficult to characterize.

The stresses mentioned so far are one dimensional in nature. The effect of these stresses on the TiSi_2 growth will most likely already be contained in the reaction coefficients. The more interesting stresses are the ones that are two or three dimensional in nature. The growth of silicides around corners will produce these types of stresses. Until now, there have been no reported results for these types of experiments. In a typical silicide structure there is the possibility of extra stresses. At the bottom corner of the spacer and Si substrate the silicide can be inhibited from sinking as the rest of the film does. This should result in the production of tensile stress in the silicide. Similarly at the top of the spacer the growing silicide can be prevented from sinking. The mechanical pinning of the Ti on top of the spacer has been used as an explanation for the bowing of silicides grown on narrow polysilicon lines [3].

2.3.3 Silicide Materials Models

During the initial first RTA step of a silicide process there are a number of materials that need to be modeled. Some of the materials are the same for the oxide system of section 2.2 but the temperatures are much lower, 600 -700 °C, for silicidation compared to 900-1100 °C for oxidation. The typical materials present in the silicide system are the oxide spacer, polysilicon gate, titanium thin films, titanium

nitride at the surface of the Ti and finally TiSi_2 . The oxide can be considered elastic but some viscous behavior may be expected for very high shear stresses. Polysilicon is not well understood as discussed in section 2.2.4 but elastic behavior is to be expected. The titanium, TiN and TiSi_2 , you would also expect to be elastic. Some viscoelastic responses might be expected for all the materials because they are thin films.

In the previous section insitu stress measurements of C49 TiSi_2 by Jongste[33] and Svilar[36] showed stress relaxation. There is obviously some viscous type behavior occurring. For the data of Svilar, using the viscoelastic model of section 2.1.2.3, a viscosity of approximately 2.8×10^{15} (dynes)(sec)/ cm^2 is needed to produce the stress relaxation. This is probably several orders of magnitude lower than even the oxide's viscosity, which is 9×10^{15} at 800 °C. The metastable C49 phase has been shown[37] to have a heavily faulted structure and a high density of defects. The formation of these defects could be due to the stress relaxation in the film. They could also provide additional diffusion paths for the diffusion of Si which has been proposed as the method of stress relaxation of C49 TiSi_2 by Jongste[33]. All of the materials in the salicide process are modeled as viscoelastic and nonlinear viscosity is available for all the models. All of the materials except TiSi_2 are modeled with very large relaxation times, until

further evidence is obtained. More experimental evidence is needed to calibrate these material models.

As in oxide growth it is possible that the extra two dimensional stress affects the growth kinetics. If the stress relaxation method is the diffusion of Si it is possible that this will either increase or decrease the amount of Si that is available to react at the Ti/TiSi₂ interface. Stress from the silicide could affect the mass transfer of Si from the substrate to the growing film. There are some indications, like the tapering of the silicide near the spacer and the poly smile, that there are some stress effects occurring. If stress is causing this behavior then it is not clear how. Just as for the material models more experiments are needed to determine these effects. Chapter 5 will describe the experiments performed in this work to try and better calibrate the silicide models in FLOOPS. Silicide thickness versus time experiments as well as experiments to determine if there are any stress effects on silicide growth will be described.

2.4 Summary

A general model for growth processes has been described. The model has two main parts, first solve for the diffusion and reaction of a reacting species and secondly account for the volume changes that occur due to the growth. A viscoelastic material model is used in this work. Stress

dependent viscosity, diffusivity and reaction rate is used to model oxidation. Stress effects seem to be evident in silicide growth but there is no clear experimental evidence of this effect. Chapter 5 will describe experiments designed to determine if there are any stress dependencies in the growth of TiSi_2 .

CHAPTER 3 MODEL IMPLEMENTATION

The implementation of the models discussed in section 2 has been done in the process simulator FLOOPS (Florida Object Oriented Processing Simulator). The software aspects of this work consist of two parts: numerics and object oriented techniques. The numerics section describes how the Finite Element Method was used to discretise the equations and how the nonlinear terms due to the stress dependencies are handled. Similarities between the models for oxide and silicide growth and the equations to be solved were taken advantage of by using object oriented techniques in their construction. This has allowed a great deal of code sharing and has decreased the development time of these models.

3.1 Numerics

The computational flowchart for the simulation of a growth process is shown in Figure 3.1. The diffusion of the reactant is solved for first. This solution is used to supply the boundary condition for flow solution. The flow is solved for and the stresses calculated. If this is a stress dependent problem a self consistent solution must be obtained. The stresses are interpolated from the integration

points to the nodes. The length of the next growth time step is then calculated. The grid is updated and the stresses are interpolated back to the integration points. For the case of nonlinear or stress dependent flow Newton's method is used to solve the nonlinear equations. The first part of this section will describe the finite element method and how it is applied to the models for oxide and silicide growth. The second part of this chapter will describe the stress interpolation. The third part of this section will describe the solution techniques used for the case of nonlinear growth.

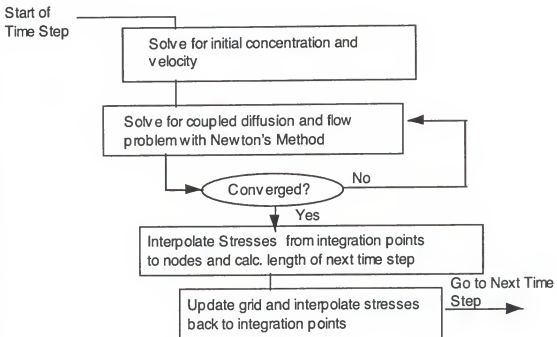


Figure 3-1: Computational flowchart for one time step of a growth process.

3.1.1.1 FEM

The finite element method (FEM) is used to solve for both the diffusion of reactant and the flow due to the volume changes. The finite element method requires the subdivision of the region into small elements. The response characteristics of each element are described in some simplified way. For infinitely small elements the solution of the problem will be exact. The general computational algorithm is shown in Figure 3-2. The first step is to break the region up into a finite number of subdomains or finite elements. Each finite element has a simple geometry and nodal points, at given coordinates, that give the elements position relative to a set of global axes. The shape of each element is defined in terms of these coordinates using interpolation or shape functions. These shape functions are also used to express the variation of the unknown inside each element. The shape functions give the variation of the unknown (for example velocity) in terms of their values at the nodal points. The next step is to find the stiffness matrix for each element. These coefficient matrices describe the response characteristics of each element. The element stiffness matrices are assembled into a global matrix that describes the behavior of the entire region. This matrix is then solved for the desired unknown, for example velocity. Once the unknowns have been solved for they are used to find the other parameters of interest like,

stresses. The major emphasis of this work has been developing the finite element code to perform steps 2, 3 and 5 in Figure 3-2. The other steps have been done by other researchers working on FLOOPS or using public domain software packages. Section 3.1.1.1 will describe the basics of the FEM while section 3.1.1.2 will describe the discretization of the diffusion equation and section 3.1.1.3 describes the application of the FEM to the flow solution for various types of material behavior.

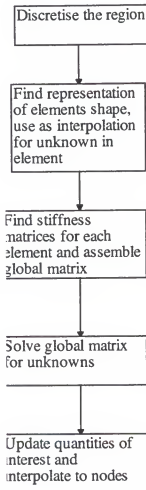


Figure 3-2: General algorithm for the finite element method.

3.1.1.1 FEM basics

As mentioned in the previous section the finite element method divides the solution region into simply shaped elements. The elements all have a certain number and order of nodes. Interpolation or shape functions are set up that specify the unknowns anywhere in the element as a function of the unknowns at the nodal points, where the unknowns will be found. The FEM uses polynomial functions that vary over elements in the domain as the shape functions. The coefficients of the shape functions are determined by the size and shape of the elements. Shape functions are chosen so that they are one at their node and zero at all the other nodes. For a scalar unknown at any point in the element is given by

$$u = N a^e \quad (3.1)$$

where for a simple 3 noded triangle with nodes i, j and m

$$u = u(x, y) \quad (3.2)$$

$$N = [N_i, N_j, N_m] \quad (3.3)$$

$$\mathbf{a}^e = \begin{Bmatrix} a_i \\ a_j \\ a_m \end{Bmatrix} \quad (3.4)$$

where N_i is the shape function at the i th node and a_i is the variable at the i th node. For most elements it is easiest to define the shape functions in terms of a generic element, for example the linear quadrilateral of Figure 3-3. The shape functions are defined in terms of the local coordinate system. The shape functions and their derivatives are then transformed to the global coordinate system. For a general three-dimensional system with global coordinate system $x, y,$

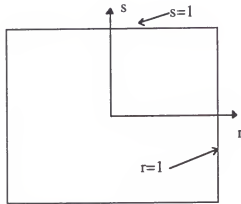


Figure 3-3: Generic quadrilateral

z and local coordinate system r, s, t we usually need to know the derivatives of the shape functions as well as the volume of the element. A coordinate x in an element e can be expressed by

$$x = \sum_{k=0}^n N_k(r,s,t) x_k^e \quad (3.5)$$

where N_k and x_k are the k th shape function and coordinate of the element and n is the number of nodes in the element. The derivative can be determined using partial derivatives, for example the derivative of the i th shape function with respect to r is

$$\frac{\partial N_i}{\partial r} = \frac{\partial N_i}{\partial x} \frac{\partial x}{\partial r} + \frac{\partial N_i}{\partial y} \frac{\partial y}{\partial r} + \frac{\partial N_i}{\partial z} \frac{\partial z}{\partial r} \quad (3.6)$$

For all three coordinates the results can be written in matrix form as

$$\begin{Bmatrix} \frac{\partial N_i}{\partial r} \\ \frac{\partial N_i}{\partial s} \\ \frac{\partial N_i}{\partial t} \end{Bmatrix} = J \begin{Bmatrix} \frac{\partial N_i}{\partial x} \\ \frac{\partial N_i}{\partial y} \\ \frac{\partial N_i}{\partial z} \end{Bmatrix} \quad (3.7)$$

where J , the Jacobian matrix, is given by

$$\begin{bmatrix} \frac{\partial x}{\partial r} & \frac{\partial y}{\partial r} & \frac{\partial z}{\partial r} \\ \frac{\partial x}{\partial s} & \frac{\partial y}{\partial s} & \frac{\partial z}{\partial s} \\ \frac{\partial x}{\partial t} & \frac{\partial y}{\partial t} & \frac{\partial z}{\partial t} \end{bmatrix} \quad (3.8)$$

The terms in equation 3.8 are found by differentiating equation 3.5. Now the derivatives in terms of the global coordinates can be determined by solving equation 3.7. The volume elements needed, $dx dy dz$ are found to be

$$dx \cdot dy \cdot dz = \det(J) dr \cdot ds \cdot dt \quad (3.9)$$

where J is again the Jacobian matrix.

In the finite element method we are usually solving differential equations over the solution domain. The equations to be solved are like those discussed in section 2.1. In general we wish to find an unknown function u that satisfies a certain set of differential equations

$$A(u) = \begin{Bmatrix} A_1(u) \\ A_2(u) \\ \vdots \end{Bmatrix} = 0 \quad (3.10)$$

over some domain Ω with certain boundary conditions

$$B(u) = \begin{Bmatrix} B_1(u) \\ B_2(u) \\ \vdots \end{Bmatrix} = 0 \quad (3.11)$$

applied on Γ , the boundaries.[38] Figure 3-4 shows an example of a general domain for a two dimensional problem.

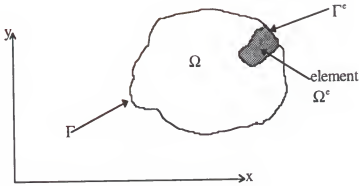


Figure 3-4 General solution domain and boundary with one example sub domain

The FEM method searches for the solution in the approximate form

$$u \approx \hat{u} = \sum_i^n N_i a_i = Na \quad (3.12)$$

where N_i is the shape function and a_i are mostly unknown, except for those specified by the boundary conditions. We now write equations 3.10 and 3.11 in an integral form[38]

$$\int_{\Omega} \mathbf{v}^T \mathbf{A}(\mathbf{u}) d\Omega + \int_{\Gamma} \bar{\mathbf{v}}^T \mathbf{B}(\mathbf{u}) d\Gamma = 0 \quad (3.13)$$

where \mathbf{v} is a set of arbitrary functions equal to the number of equations. If equation 3.13 is satisfied for all \mathbf{v} it is equivalent to satisfying equations 3.10 and 3.11. Usually we

are able to perform integration by parts on equation 3.13 to get the "weak form" of the equations

$$\int_{\Omega} C(v)^T D(u) d\Omega + \int_{\Gamma} E(\bar{v})^T G(u) d\Gamma = 0 \quad (3.14)$$

Operators **C** and **E** contain lower order derivatives than those in **A** and **B** and equation 3.14 is known as the "weak form" because it is more permissive than equation 3.13. In the Galerkin method of the FEM **v** is replaced with weighting functions, which are chosen to be the shape functions **N**. So the function to be solved for F_N is written as

$$F_n = \int_{\Omega} C(N_i)^T D(u) d\Omega + \int_{\Gamma} E(N_i)^T G(u) d\Gamma = 0 \quad (3.15)$$

where $i=1$ to n and n is the number of unknown parameters a_i . This leads to n equations and n unknowns. The most general method for solving these equations is Newton's method. For a linear partial differential equation Newton's method will give the answer in one iteration. Newton's method is given by

$$\left[\frac{\partial F_N}{\partial a_i} \right] [\Delta a_i] = -[F_N] \quad (3.16)$$

where Δa_i is the update and $\left[\frac{\partial F_N}{\partial a_i} \right]$ is the Jacobian or left hand side.

The differential equations and boundary conditions of equations 3.10 and 3.11 are now expressed as equation 3.14 which contain global integrals. These global integrals can be written as a sum of integrals over the finite elements. For example the first integral in equation 3.15 is

$$\sum_{\Omega} \int_{\Omega^e} C(N_i)^T D(u) d\Omega^e \quad (3.17)$$

Where the integral is over the area of the element. Using equation 3.12 in the element integral in equation 3.17 gives

$$\sum_{k=0}^n a_k \int_{\Omega^e} C(N_i)^T D(N_k) d\Omega^e \quad (3.18)$$

When this is used in equation 3.16 the contribution to the global Jacobian, from each element, for a linear PDE is

$$K^e = \int_{\Omega^e} C(N_i)^T D(N_k) d\Omega^e \quad (3.19)$$

The boundary terms are treated similarly.

The element stiffness integrals, such as equation 3.19, are evaluated numerically. For example

$$K^e = \sum_{p=1}^P \left[C(N_i(p))^T D(N_k(p)) dx dy dz \right] w_p \quad (3.20)$$

where P is the number of integration points of the element, $N_x(p)$ are the shape functions evaluated at the integration points, w_p is the integration weight and $dx dy dz$ is the volume of the element. If the element is mapped from a local coordinate system the volume term will be given by equation 3.9.

This section has described the general solution procedure for the FEM. In the sections to follow the specifics of how the diffusion and flow equations are solved will be described. The weak forms of each problem will be given and the element stiffness matrix will be described as well as the integration scheme used.

3.1.1.2 Diffusion

The general model for diffusion of reactant in FLOOPS is given in section 2.1.1. The specifics of the oxide and silicide systems are shown in Figures 2.5 and 2.8. In both systems the diffusion of reactant is modeled by solving the steady state diffusion equation

$$\nabla \cdot (DVC) = 0 \quad (3.21)$$

over the solution domain with specified boundary equations. As mentioned in the previous section in the FEM we start by specifying the "weak" form of the problem which is given by

$$\int_{\Omega} \nabla N_i \cdot (D \nabla C) d\Omega = \int_{\Gamma_1} N_i k_s C d\Gamma_1 + \int_{\Gamma_2} N_i k_t (C^* - C) d\Gamma_2 \quad (3.22)$$

where N_i are the shape functions and the right hand side terms are due to the boundary conditions. We now have an equation in the form of equation 3.17. By using $C = \sum N_j a_j$ we can determine the element contributions to the global Jacobian and right hand side using the same procedure as in equations 3.17 - 3.19. They are

$$\int_{\Omega^e} \nabla N_i D \nabla N_j d\Omega^e - \int_{\Gamma_1^e} N_i k_s N_j d\Gamma_1^e - \int_{\Gamma_2^e} N_i k_t (C^* - N_j) d\Gamma_2^e = 0 \quad (3.23)$$

These integrals are evaluated numerically as stated before. The elements used by FLOOPS are in two dimensions linear triangles and in three dimensions linear tetrahedra.

3.1.1.3 Flow

In the flow equations the unknowns are the nodal velocities and the equation governing deformation is Newton's second law. Newton's second law for our problems, for which body forces and acceleration are negligible [6], is

$$\frac{\partial \sigma_{ij}}{\partial x_i} = 0 \quad (3.24)$$

In equation 3.24 the confusing Einstein summation is used which means that the indices run over the number of dimensions. So written in matrix form for a three dimensional problem equation 3.24 is

$$\left\{ \begin{array}{ccc} \frac{\partial \sigma_{xx}}{\partial x} & \frac{\partial \sigma_{xy}}{\partial y} & \frac{\partial \sigma_{xz}}{\partial z} \\ \frac{\partial \sigma_{yx}}{\partial x} & \frac{\partial \sigma_{yy}}{\partial y} & \frac{\partial \sigma_{yz}}{\partial z} \\ \frac{\partial \sigma_{zx}}{\partial x} & \frac{\partial \sigma_{zy}}{\partial y} & \frac{\partial \sigma_{zz}}{\partial z} \end{array} \right\} = 0 \quad (3.25)$$

Going through similar steps as for the diffusion equation, we get the "weak" form of the flow equations which is called the virtual work equation. It is given by

$$\int_{\Omega} \delta \dot{\epsilon}^T \sigma d\Omega = 0 \quad (3.26)$$

where $\delta \dot{\epsilon}$ is the virtual strain rate and σ is the stress tensor. The unknown velocities are given by

$$u = \sum N_i a_i \quad (3.27)$$

The strain rate and stress tensors are written in vector form as

$$\dot{\epsilon} = \begin{Bmatrix} \dot{\epsilon}_{xx} \\ \dot{\epsilon}_{yy} \\ \dot{\epsilon}_{zz} \\ \dot{\epsilon}_{xy} \\ \dot{\epsilon}_{yz} \\ \dot{\epsilon}_{zx} \end{Bmatrix}, \quad \sigma = \begin{Bmatrix} \sigma_{xx} \\ \sigma_{yy} \\ \sigma_{zz} \\ \sigma_{xy} \\ \sigma_{yz} \\ \sigma_{zx} \end{Bmatrix} \quad (3.28)$$

where the strain rate is the derivative of the velocity for example

$$\dot{\epsilon}_{xx} = \frac{\partial u_x}{\partial x} \quad \text{and} \quad \dot{\epsilon}_{xy} = \frac{\partial u_x}{\partial y} + \frac{\partial u_y}{\partial x} \quad (3.29)$$

But since the velocity is given by equation 3.27 the strain rate is the derivative of the shape functions times the unknowns. The stress is related to the strain rate through the constitutive relationships of section 2.1.2. For a viscous material the strain rate to stress relationship is given by equation 2.13. The D matrix in equation 2.13 is

$$D = \begin{Bmatrix} C_1 & C_2 & C_2 & 0 & 0 & 0 \\ C_2 & C_1 & C_2 & 0 & 0 & 0 \\ C_2 & C_2 & C_1 & 0 & 0 & 0 \\ 0 & 0 & 0 & C_3 & 0 & 0 \\ 0 & 0 & 0 & 0 & C_3 & 0 \\ 0 & 0 & 0 & 0 & 0 & C_3 \end{Bmatrix} \quad (3.30)$$

where C_1 , C_2 and C_3 are functions of viscosity and Poisson's ratio. The element stiffness matrix can now be written as

$$K^e = \int_{\Omega_e} B^T D B d\Omega_e \quad (3.31)$$

where B is the derivative of the shape function matrix. This element stiffness matrix is again evaluated numerically. The three dimensional elements used are linear tetrahedral.

3.1.1.3.1 Two dimensional plane strain

The above relationships are for three dimensional viscous analysis. For a two dimensional problem certain assumptions must be made to solve the problem. One typical method, and the method used here, is to choose the plane strain approximation that the material is infinitely deep along the z axis. This changes the stress and strain rate tensors to

$$\dot{\epsilon} = \begin{Bmatrix} \dot{\epsilon}_{xx} \\ \dot{\epsilon}_{yy} \\ \dot{\epsilon}_{xy} \end{Bmatrix} \quad \text{and} \quad \sigma = \begin{Bmatrix} \sigma_{xx} \\ \sigma_{yy} \\ \sigma_{xy} \end{Bmatrix} \quad (3.32)$$

The D and B matrices also change accordingly. The two dimensional elements supported are linear and quadratic triangles.

3.1.1.3.2 FEM velocity-pressure

When the discretization of sections 3.1.1.3 and 3.1.1.3.1 are applied to the problem of incompressible or nearly incompressible materials the method fails or produces

oscillatory results.[38] One approach to solve this problem is to use a mixed formulation where you solve for the velocity and pressure seperaately. The basic technique is to break the stress into it's hydrostatic and deviatoric parts

$$\sigma = \sigma_d - mp \quad (3.33)$$

where $m = [1 \ 1 \ 1 \ 0 \ 0 \ 0]$, p is the hydrostatic pressure and σ_d is the deviatoric stress. Equation 3.33 is used in equation 3.26 with a second equation relating the pressure to the strain rate

$$m^T \dot{\epsilon} - \frac{p}{K} = 0 \quad (3.34)$$

where K is the bulk modulus, are discretised to give the element stiffness matrix. It is

$$\begin{bmatrix} A & C \\ C^T & V \end{bmatrix} \begin{Bmatrix} u \\ p \end{Bmatrix} = \begin{Bmatrix} f_1 \\ 0 \end{Bmatrix} \quad (3.35)$$

where

$$A = \int_{\Omega^e} B^T \mu \bar{D} B d\Omega^e \quad (3.36)$$

$$C = - \int_{\Omega^e} B^T m N_p d\Omega^e \quad (3.37)$$

$$V = \int_{\Omega^e} \frac{N_p N_p}{K} d\Omega^e \quad (3.38)$$

In the above equations N_p is the shape functions for the pressure and

$$\bar{D} = \begin{bmatrix} 4/3 & -2/3 & -2/3 & 0 & 0 & 0 \\ -2/3 & 4/3 & -2/3 & 0 & 0 & 0 \\ -2/3 & -2/3 & 4/3 & 0 & 0 & 0 \\ 0 & 0 & 0 & 1 & 0 & 0 \\ 0 & 0 & 0 & 0 & 1 & 0 \\ 0 & 0 & 0 & 0 & 0 & 1 \end{bmatrix} \quad (3.39)$$

The key point of the velocity pressure formulation is to use lower order integration on the pressure part of the element. This formulation has been used in FLOOPS on 6/1 triangles. This means that quadratic shape functions are used for the velocities and the pressure is constant across the element.

3.1.1.3.3 Viscoelastic flow

The FEM formulation in section 3.1.1.3 is for viscous behavior. The second and more useful model in FLOOPS is the viscoelastic model described in section 2.1.2.3 with or without nonlinear viscosity. The FEM described can be used to model viscoelastic behavior by including the correct constitutive expression. Using the notation of the above

section for a velocity-pressure formulation the correct constitutive relationships are for the deviatoric stress

$$\sigma_d = \mu \left(1 - e^{\frac{-\Delta t}{\tau}} \right) \overline{D}\dot{\epsilon} + \sigma_{d0} e^{\frac{-\Delta t}{\tau}} \quad (3.40)$$

and for the dilatational or pressure component

$$p = K\Delta t m^T \dot{\epsilon} + p_0 \quad (3.41)$$

In these equations $\mu \left(1 - e^{\frac{-\Delta t}{\tau}} \right)$ is the effective viscosity, σ_{d0} and p_0 are the residual stresses from the last time step and $\tau = \frac{\mu}{G}$ is the relaxation time constant. The residual stresses are treated as right hand side terms of the form

$$\int_{\Omega^e} B^T \sigma_0 d\Omega^e \quad (3.42)$$

This model is very useful because stress terms due to other sources, like thermal mismatch, can be included in the same way. Viscoelastic models are used in FLOOPS in both velocity-pressure and velocity formulations. The velocity formulation is the most used formulation. It is used for all the nonlinear formulations discussed in section 3.1.3.

3.1.1.4 Boundary conditions for flow solution

There are three main boundary conditions used in the flow solution as well as special handling of triple points. Triple points are where three or more materials come together at the same point. The boundaries are depicted in Figure 3-5, a TiSi_2 growth example. In FLOOPS, there are three nodes at each interface. For the case of a growing interface there is a node for the growing material (TiSi_2), a node for the consuming material (Silicon, Titanium) and a node for the interface mesh (a mesh of $n-1$ dimension, where n is the dimension of the simulation). The boundary conditions need to account for the volume changes and how the nodes are ultimately moved.

The reflecting boundary condition is used at the edges of simulations. This boundary condition states that the normal component of the velocity at this interface is zero. This boundary condition implies that the structure is the same or reflected on both sides of the interface. In two dimensions this allows us to simulate $1/2$ of the structure and in three dimensions this allows the simulation of $1/4$ of the structure.

The consume boundary condition is used at silicon and growing material interfaces. This boundary condition accounts for the consumption of silicon due to the reaction, as well as accounting for the volume change at the interface. For the case of SiO_2 growth the boundary condition used

accounts for the volume expansion due to formation of SiO_2 . This is accomplished by assigning the velocity for the silicon consumption to the silicon node, the volume expansion is applied as a Dirichlet boundary condition on the SiO_2 node. After the material flow has been solved for, all three nodes at the interface are moved according to the silicon node velocity. For the case of TiSi_2 simulation both the silicon and TiSi_2 nodes get velocities for the consumption of silicon. This is because there is no volume expansion at this interface. This boundary condition implies that there are no voids formed at the TiSi_2 and silicon interface. The main assumption of this boundary condition is that the silicon is a rigid body. This is a good assumption considering the high Young's modulus of silicon as well as the thickness of the wafer in comparison to the thickness of the films of interest. The result of this boundary condition, instead of the consume and flow boundary condition, is much less CPU time and memory intensive because there is no need to solve for the flow equations in the silicon. This is important when considering the simulation of three dimensional LOCOS structures.

The consume and flow boundary condition is needed for any growing interface where the material can not be considered a rigid body. In this case the volume expansion is accounted for by solving for an extra equation that specifies that the difference between the growing material and the material being consumed (polysilicon or titanium)

velocities is the volume expansion at the interface. Once the flow has been solved for the the consumption velocity is added in and the nodes moved.

Triple points, for example where the SiO_2 spacer, TiSi_2 and silicon meshes come together are difficult to handle. The method of dealing with triple points in this work is to direct the velocity at the triple point down the interface of the non growing and consuming interface (silicon and SiO_2). This makes it easier for the moving boundary code to handle these points. No special techniques need to be used to try and find when the nodes have been overrun.

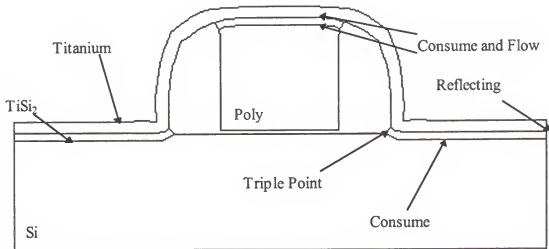


Figure 3-5: Salicide structure demonstrating the different boundary conditions used in simulating material flow.

3.1.2 Stress Interpolation

One important consideration in the viscoelastic model is how to handle the residual stresses from time step to time step on a moving grid. The stresses are computed before the grid is moved so that if in moving the grid the elements are rotated there will be an error in the residual stresses. The way to handle this problem is to rotate the stresses before the grid is moved so that the stresses will be correct on the updated grid. In two dimensions this was taken into account by determining the angle of rotation of the elements and then rotating the stresses using this angle. Simulations were run with and without correcting for this error and compared. The differences were minor, less than a 5 percent difference in the birds beak height and length for the worst case. Due to the fact that this is below the resolution of the measurement of these features and the fact that implementing this algorithm in three dimensions would be difficult and computationally inefficient, stress rotation is not used for the oxide growth simulations in this work.

During solution the flow equations the stresses are known only at the integration points of the elements, the center of a linear triangle or tetrahedral. These stresses need to be interpolated to the nodes for plotting as well as so they are useful to other simulation steps, like calculating the stress in silicon, using the stresses to couple to the reaction rate boundary condition, or most

importantly, so the grid can be moved and updated. The method used to interpolate the stresses is a simple one. The stress at a node is the average of the stresses of all of the elements (either tetrahedral or triangles) that the node is attached.

3.1.3 Nonlinear and Stress Dependencies

In Figure 3-1 there is a loop which is used when the stress dependent terms are used in a simulation. In an oxidation there are three stresses used by the nonlinear terms the normal stress at the Si/SiO₂ interface, the pressure in the oxide and the maximum shear stress. There are two main techniques for solving the nonlinear iterations, Successive Over Relaxation (SOR) and Newton's Method. Both approaches have been tried in FLOOPS and Newton's method has been found to be more robust, especially for three-dimensional simulations.

3.1.3.1 Successive over relaxation

The nonlinear iterations were originally solved with a numerical relaxation technique[15,19]. The diffusion and flow equations are solved alternately with the values calculated from the other step. The stresses which cause the nonlinear terms are numerically relaxed before they are used

in the stress dependent terms. For example consider the pressure at the nth iteration

$$P_n = P_n \omega + P_{n-1}(1 - \omega) \quad (3.42)$$

where $\omega \leq 1$ and is adapted from iteration to iteration. If the error has decreased from the last time step it is increased, while if the error has increased it is decreased. Convergence is obtained where the relaxed terms from one time step to the other are small or

$$\text{err} = \frac{\sum s_n - s_{n-1}}{N_s} \leq \text{tol} \quad (3.43)$$

where s are the stresses being relaxed and N_s is the number of stresses being relaxed.

Including the elastic effect is beneficial for this technique. In fact trying to use this on a viscous incompressible problem is extremely time consuming. Grid quality is critical for this nonlinear iteration scheme. The most important points are to avoid high aspect ratio and unevenly sized triangles. The grid in FLOOPS is not remeshed between time steps as done by Senez[19]. Grid quality is maintained by splitting edges in the middle when new grid needs to be added. This helps prevent high aspect ratio triangles from forming. A second technique for helping convergence is to make each oxide grid points' position the

average of it's neighbors. In tests this technique has greatly improved performance without loss of accuracy. Unfortunately the grid quality in the three dimensional meshes in FLOOPS are not as high as in two dimensions. This causes convergence problems and has led us to search for a more stable method.

3.1.3.2 Newton's method

Due to the fact that the Newton's method based scheme implemented by Rafferty worked so well for viscous incompressible simulations, while the SOR method did not, a Newton's method based scheme was implemented. Newton's method is given by equation 3.16. In using this method for a

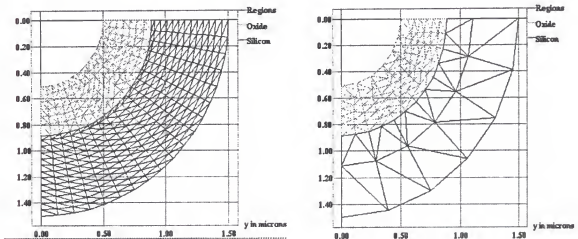


Figure 3-6: Oxide growth simulations on hole structure. Left high grid quality case, right lower grid quality.

nonlinear growth simulation a coupled system of both the concentrations and velocities need to be solved. This is, of

course, much harder to implement because derivatives need to be calculated for the Jacobian. The implementation of this method for nonlinear stress dependent growth simulations will be discussed in section 3.1.4.

3.1.3.3 Comparisons for grid

To test whether Newton's method is more robust than SOR a numerical experiment was carried out on identical structures: one gridded with high quality triangles and the other allowing the grid quality to worsen. On these structures stress dependent oxidation simulations of oxide growth in a hole were simulated using either Newton's method or SOR. The completed simulations are shown in Figure 3.6. Newton's method with continuation (λ starting at 0.25) was used. Convergence was obtained when the L_2 norm of the velocities was less than $1e-6$. For SOR with adaptive relaxation, convergence was obtained when error was less than $1e-3$. The test example was of a hole etched in Si with radius = 0.72 μm . The oxide growth was 1100 °C 40 minute wet oxidation. Stress dependent diffusivity and viscosity only were used in the simulations. The convergence history versus time step for all four simulations is shown in Figure 3.7. As can be seen the SOR method is much more sensitive to grid quality than is the Newton's method. This does not mean that Newton's method is insensitive to grid quality, just less sensitive. Due to these results it was decided that Newton's method was a much better approach to use for the

simulation of stress dependent growth processes. The main reason is that in three-dimensional simulations and silicide growth simulations the grid quality is usually much lower than in the two-dimensional LOCOS simulations.

SOR vs Newton's Method

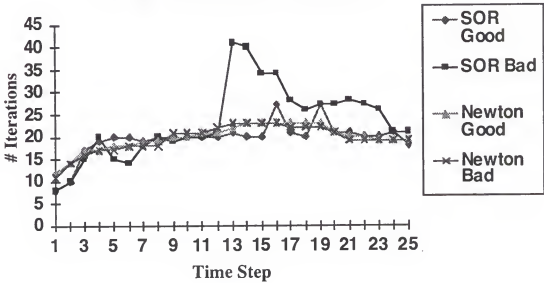


Figure 3-7: Comparison of the convergence pattern of both SOR and Newton's method versus the time step.

3.1.4 Implementation of Newton's Method

Newton's method is given by equation 3.16 repeated here

$$\left[\frac{\partial F_N}{\partial a_i} \right] [\Delta a_i] = -[F_N] \quad (3.16)$$

where Δa_i is the update and $\left[\frac{\partial F_N}{\partial a_i} \right]$ is the Jacobian or left hand side. The solution variable after each iteration is given by $a_{i+1} = a_i + \Delta a_i$. The subscripts refer to the variable at the i th and $i+1$ iterations. Two main methods to speed convergence have been implemented; continuation and damping[6]. In damping the update is scaled by some factor α

$$a_{i+1} = a_i + \alpha * \Delta a_i \quad 3.44$$

until the right hand side (rhs) at the new solution is less than the rhs at the old solution $F_N(a_{i+1}) < F_N(a_i)$. Unfortunately the value of α needed to reduce the rhs is sometimes too small to be useful. The smallest value of α allowed in FLOOPS is 0.125. When the α needed to reduce the rhs is less than 0.125, continuation is used.

Continuation is used to find a better initial guess for the Newton iterations. The initial guess used in FLOOPS is the diffusion and flow solutions with the stress dependencies turned off. When continuation is used the activation volumes for the stress dependent terms are expressed as $V_x = \lambda V_{x_0}$. Here λ is some value less than 1.0. λ is decreased until convergence is obtained, then it is increased until $\lambda=1$. When continuation is used it is equivalent to solving a less

stress dependent problem and using that solution as an initial guess to a stronger (higher λ) problem. The combination of continuation and damping has lead to a very robust iterative method.

The specifics of the Newton's method used is similar to Rafferty[6]. The main difference is in the derivative terms due to the stress dependent viscosity used in the viscoelastic model and the handling of boundary terms such as those due to the stress dependent reaction rate. In the growing material both the velocities(x,y,z) and concentration of reactant must be solved for at each node. For materials that are deforming only the velocities must be solved for at each node. The derivatives of the right hand side are taken with respect to each solution variable.

The main difference between this and Rafferty's work is that when the Eyring or stress dependent viscosity is used in the viscoelastic stress to strain rate relationship it can not be inverted. To find $d\sigma/d\epsilon$, an inner SOR loop is needed to find a self consistant stress and strain rate. The $d\sigma/d\epsilon$ are stored and used whenever they are needed. For bulk elements the D matrix in equation 3.31 for the flow model is exactly $d\sigma/d\epsilon$. For the derivatives of terms due to the diffusion of reactant, equation 3.21, the only term dependent on the velocity is the diffusivity D. The derivatives of the

diffusivity becomes $(dD/d\sigma) \cdot (d\sigma/d\varepsilon) \cdot (d\varepsilon/du)$, where $d\varepsilon/du$ is just the B matrix from equation 3.31. Similarly terms due to the k_s dependence on stress are evaluated as $(dk_s/d\sigma) \cdot (d\sigma/d\varepsilon) \cdot (d\varepsilon/du)$. Since this is a boundary term on the interface not in bulk elements the derivatives at the interface are evaluated at each element attached to the node on the interface. So at an interface node the derivatives are given by

$$\frac{dk_s}{du} = \sum_N \frac{dk_s}{d\sigma} \cdot \frac{d\sigma}{d\varepsilon} \cdot \frac{d\varepsilon}{du} \quad 3.45$$

where N is the number of elements (either triangles or tetrahedra) attached to the boundary node. For the boundary nodes the stresses are not averaged to the nodes. Effectively the reduction due to the stress and the derivatives are averaged in the final global matrix.

3.2 Object-Oriented Techniques

In the previous sections there have been many similarities between the oxide and silicide systems as well as the FEM techniques used to solve the diffusion equation and the various deformation models. The object oriented nature of FLOOPS was used to take advantage of these similarities. This has allowed code sharing and has sped the development of the various models. The remainder of this

chapter will describe the general classes applied to the physics and numerics already described in chapter 2 and the beginning of Chapter 3.

3.2.1 Silicide/Oxide Physics

Referring back to section 2.1.1 the general diffusion/reaction system that was applied to both the silicide and oxide systems consisted of three main parts: first there was a mass transfer interface, second there was a constant diffusion layer and third there was a reacting interface. In FLOOPS there are general classes which are used to model each type of behavior. These classes are applied to silicidation and oxidation as shown in Table 3-1.

Table 3-1: Analogy between growth models in FLOOPS

Growth Model	Reactant Source	Constant Diffusion	Reacting Surface
SiO_2	Gas/ SiO_2 interface	SiO_2	Si/ SiO_2 interface
TiSi_2	Si/ TiSi_2 interface	TiSi_2	TiSi_2 / Ti interface
TiN	Gas/ TiN interface	TiN	TiN/ Ti interface

The only differences is the parameter classes from which the coefficients for the growth, like diffusivity, mass transfer coefficient and reaction rate are taken from. In fact these parameter classes also share much of the same code.

For the deformation problems there is a similar analogy. There are materials that are consumed, materials that flow and materials that must flow while being consumed. Table 3-2 shows these general models and how they are applied to modeling silicidation and oxidation. The same parameter classes are used to calculate the applied velocities for the consuming classes. A flow parameter class is used for the material coefficients like Young's modulus, Poisson's ratio and viscosity.

Table 3-2: Similarities between material models in silicide and oxide growth.

Growth System	Consumed	Flow	Consume and Flow
SiO_2	Si	SiO_2 , Si_3N_4	Poly
TiSi_2	Si	TiSi_2 , SiO_2	Poly, Ti
TiN	—————	TiN	Ti

3.2.2 FEM Numerics

Object-oriented techniques were also used for the finite element code. There is a base class that contains the shape function information and derived classes for each of the problems solved. This is shown in Figure 3-8. There are classes for velocity-pressure and velocity formulations for the flow problem, the diffusion of reactant, and velocity relaxation. Velocity relaxation is used by the grid code to keep even grid spacing for three-dimensional oxide growth.

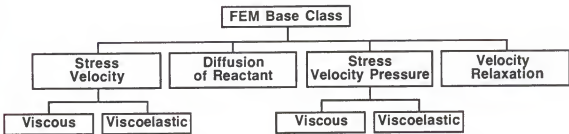


Figure 3-8: FEM class structure in FLOOPS.

This has allowed three dimensional oxide simulations to be run while the moving boundary grid code was being developed. Creating the velocity relaxation code took less than two days of work, which shows the power of object oriented programming. The classes at this second level assemble the element stiffness matrices from matrices of the shape functions or their derivatives, like the B matrix from the base class and matrices that are dependent on the exact material model like the D matrix and right hand side. The D

matrix will change for all of the third level of classes and there will be right hand side terms only for the viscoelastic models. These classes also calculate the stresses from the solution in a similar manner.

3.3 Summary

This chapter has described the numerical and software techniques used to implement the models described in chapter 2. The Finite Element Method is used to solve for the diffusion and reaction of reactant as well as for the deformation and flow due to the volume change of the reaction. Several different methods for solving the flow equation have been tried. Linear shape functions are used in two and three dimensions. The best method was found to be a velocity formulation of the viscoelastic model. Newton's method was found to be the best method to use to solve the nonlinear equations that arise due to stress dependent growth. Object oriented methods were used throughout the development of these models. This has led to a good deal of code sharing and decreased development time.

CHAPTER 4

ONE-DIMENSIONAL SILICIDE SIMULATIONS AND EXPERIMENTS

4.1 Simulation of Titanium Silicide Reaction Kinetics

The simulation of TiSi_2 growth kinetics is important for any process simulation program. The shape and stress of the silicide can not be accurately simulated if the thickness versus time can not accurately be simulated. In addition any simulation of vacancy injection during silicide growth will need accurate thickness versus time simulation. There are two main methods for performing the first anneal of a silicide process. The first method is a furnace anneal and the second is to use a rapid thermal anneal (RTA). Both methods are performed in an Nitrogen ambient to prevent bridging of the spacer. This section will use the reaction diffusion model of chapter 2 to model the reaction of titanium and silicon annealed in a furnace as well as an RTA.

4.1.1 Furnace Annealing of Titanium and Silicon

4.1.1.1 Overview of Experiment

Pico[24] designed and carried out an experiment to investigate the growth kinetics of TiSi_2 on silicon. The starting material was lightly doped, approximately $10 \text{ } \Omega\text{cm}$, p type $\langle 100 \rangle$ Si wafers. The substrates were then cleaned. The wafers were then quickly loaded into the deposition chamber and pumped down to 10^{-6} Torr within 3-4 minutes. The evaporator was then pumped down to between 4×10^{-8} and 9×10^{-8} . Titanium was then electron-beam evaporated onto the substrate. The thickness of the films was between 70 and 300 nm. The samples were then annealed at $470\text{--}650^\circ\text{C}$ in a tube furnace for times ranging from 20 minutes to several hours. In order to determine the reaction kinetics the 300 nm Ti on Si samples were analyzed to determine silicide phase presence and formation.

The analysis of the samples to determine the composition and thickness silicide was performed using Auger electron spectroscopy (AES) depth profiling, Read camera x-ray diffraction (XRD) and transmission electron microscopy (TEM). The AES results were complemented by x-ray photoelectron spectroscopy (XPS) and Rutherford backscattering (RBS) measurements.

4.1.1.2 Experimental Results

AES analysis of the as deposited Ti films showed low, less than 1-2%, O and C impurities in the bulk of the film. The oxygen concentration was higher near the top surface, ~5%. The annealed samples showed a Ti/precursor/TiSi₂/Si structure. Both the precursor and disilicide film grew as long as there was unreacted titanium remaining up until the last 100-300 angstroms where the oxygen in the system was snowplowed. Once the titanium layer stops reacting the TiSi₂ layer continues to grow at the expense of the TiSi precursor layer. No TiSi₂ growth was seen for samples annealed below 500 °C. In partially reacted samples the remaining Ti film contains up to 15 percent oxygen. The integrated oxygen concentration is much higher then in the deposited samples. This oxygen contamination is presumably from the anneal step. The oxygen does not seem to inhibit the reaction except in the last 100-300 angstroms of titanium.

The rate of TiSi₂ growth for 300 nm thick Ti on <100> Si is measured using AES. The results are plotted in Figure 4-1. The TiSi₂ formed parabolically with time indicating that the growth is diffusion limited. The total silicide thickness, TiSi+TiSi₂, also exhibits diffusion limited growth.

4.1.1.3 Modeling of Results

The general growth model of chapter 2 is used to model the growth of TiSi₂. The silicide growth data shown in Figure

4-1 indicate that the rate limiting step is the diffusion of silicon. This causes equation 2.7 to reduce to

$$x^2 = B \cdot t \quad (4.1)$$

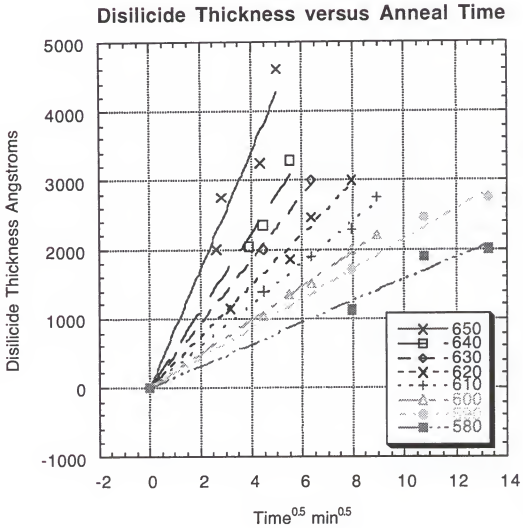


Figure 4-1: Disilicide thickness versus time. Data from Pico[24].

where B is the parabolic growth coefficient from equation 2.7

$$B = \frac{2DC^*}{N_1} \quad (4.2)$$

where D is the diffusivity of Si in the silicide, C^* is the concentration of reactant at the silicide silicon interface and N_1 is the number of molecules of reactant incorporated into a unit volume of growing silicide. N_1 is calculated to be 4.4×10^{22} Si/cm³. Unfortunately, C^* and D can not be determined independently. Only their product can be found. Equation 4.1 is used to fit the data in Figure 4-1 at each temperature. The parabolic coefficient can be expressed as

$$B = B_0 \exp\left(\frac{-E_a}{kT}\right) \quad (4.3)$$

here B_0 is the preexponential, E_a is the activation energy, k is Boltzman's constant and T is the temperature in degrees Kelvin. The natural log of parabolic coefficient for each temperature is then plotted versus the inverse temperature to determine the activation energy of the reaction. Pico found this activation energy to be 2.5 ev. B_0 is then determined to be 1.55×10^{11} um²/min.

Using the fit in equation 4.3, FLOOPS is used to simulate the data in Figure 4.1. The simulated growth curves compared to data are shown in Figure 4.2. Here the graphs are of TiSi₂ thickness in microns versus time in minutes. The

fit to the data is good. The 650 °C data is not as close a fit but B_0 can be increased to $2.75e11$ to give the fit shown in Figure 4.3.

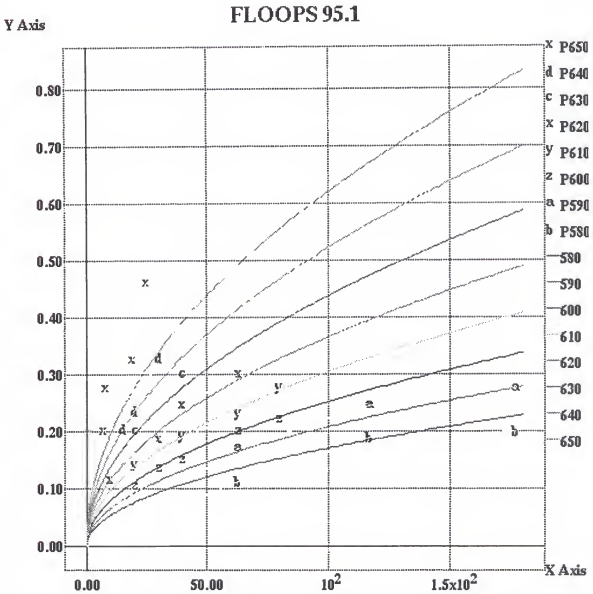


Figure 4-2: Comparison to data of simulation of disilicide thickness in μm versus anneal time in minutes.

4.1.2 Furnace Annealing of Titanium and Amorphous Silicon

4.1.2.1 Overview of Experiment

Hung[23] designed and implemented an experiment into the growth kinetics of TiSi_2 on amorphous silicon. The starting

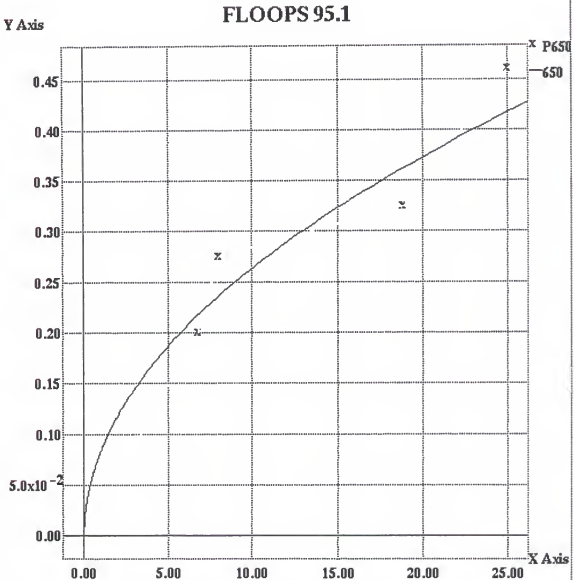


Figure 4-3: Readjusted simulation of 650 silicide thickness versus time compared to data.

substrate is <100> silicon. The wafers were cleaned and then etched in dilute HF immediately prior to loading into a vacuum system. Titanium was then electron gun deposited onto the samples, followed by the evaporation of amorphous Si [α -Si]. The α -Si was deposited before breaking the vacuum. The vacuum during deposition was lower than 5×10^{-7} Torr. Some samples had a stack consisting of Si/SiO₂/ α -Si/Ti.

All the samples were annealed in a vacuum furnace at $\sim 5 \times 10^{-7}$ Torr, with varying times and temperatures. MeV ⁴He backscattering spectrometry and x-ray diffraction were used to characterize the samples and determine the growth kinetics of the growing layers.

4.1.2.2 Experimental Results

The reaction of the Ti with α -Si is found to react faster than with substrate Si. Figure 4.4 shows the TiSi₂ thickness versus (time)^{1/2} for the α -Si/Ti reactions. This reaction is also diffusion limited as shown by the linear dependence of thickness on (time)^{1/2}. The phase present in this reaction is reported to be TiSi₂ only. The substrate silicon with Ti reaction results were not reproducible and no thickness versus time data is reported. This is believed to be due to the presence of oxygen and other impurities at the Ti/Si interface. The Ti/ α -Si interface is much cleaner due

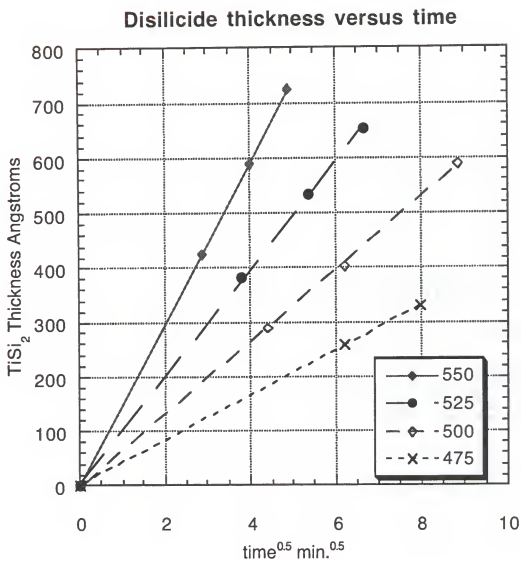


Figure 4-4: Disilicide thickness versus anneal time, data from Hung[23].

to the deposition of the Ti and amorphous Si without breaking the vacuum during the evaporation. When α -Si deposited samples were exposed to the ambient for a day, cleaned in the same manner as the crystal Si samples, and

then annealed they displayed reaction kinetics similar to the Ti/substrate silicon samples.

4.1.2.3 Modeling of Results

The method of section 4.1.1.3 is also applied to the

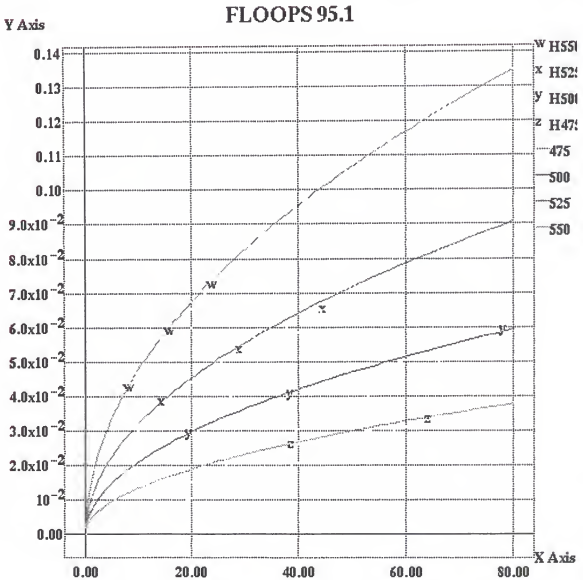


Figure 4-5: Simulated thickness versus time curves compared to data.

data of Figure 4.4. Equation 4.1 is fit to the data at each temperature. The rate coefficient is then fit to the Arrhenius equation of equation 4.3. The activation energy is 1.8 eV and the pre-exponential factor is $2.16 \times 10^7 \text{ um}^2/\text{min}$. Figure 4.5 shows the FLOOPS simulations using these values. The plot is of TiSi_2 thickness versus time in minutes. The simulations do a very good job of fitting the data.

4.1.3 Rapid Thermal Annealing of Titanium and Silicon

4.1.3.1 Overview of Experiment

Lanerolle[39] designed and implemented an experiment investigating the rapid thermal annealing of titanium and silicon samples. The starting substrates were lightly doped, 2-30 $\Omega \text{ cm}$ p-type <100> silicon. The samples were then cleaned and etched in 40:1 buffered HF to remove any residual oxide. Some of the films were doped with either a $5 \times 10^{15} \text{ ions/cm}^2$ 120 keV arsenic implant or $3.7 \times 10^{15} \text{ ions/cm}^2$ of boron at 45 keV. Titanium films of between 200 and 1000 Å were then sputtered onto the samples. The rapid thermal anneals (RTA) were carried out in two steps using an A.G. Associates model 2101 rapid thermal processing system. The first step was for times between 5 and 100 seconds and temperatures between 450 and 750 °C. The annealing ambient was either argon or nitrogen. After the first RTA the samples were given a selective etch to remove any remaining Ti and TiN that

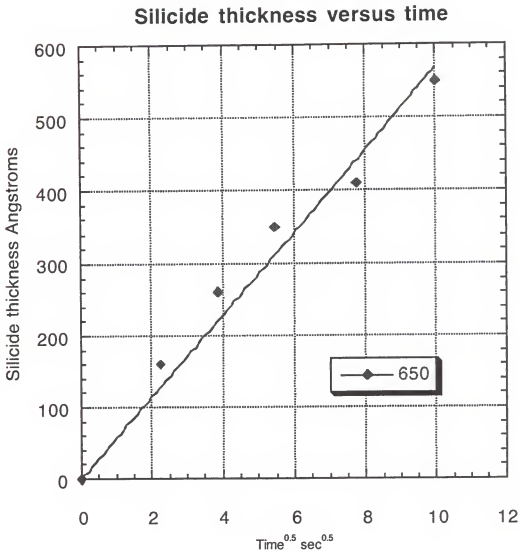


Figure 4-6: Silicide thickness versus RTA time at 650 °C.

formed. After the selective etch the samples were given a second RTA of 30 seconds at 850 °C.

Thickness measurements were taken after the first RTA, selective etch and the second RTA. The film thickness was measured by masking an area with photoresist and etching the silicide with HF. The film thickness was measured using a

Tencor Instruments Alpha Step profilometer. Unfortunately it is hard to determine which phases of titanium silicide are present in the film being measured. After the second RTA the silicides have probably been converted to C54 TiSi_2 .

4.1.3.2 Experimental Results and Modeling

There is a large amount of qualitative data on silicide growth. The rate of reaction in argon ambient is faster than in nitrogen. Doped silicon reacts slower than undoped silicon. Unfortunately there is very little thickness versus time data like those in the previous two sections. The only data of this type from the paper is shown in Figure 4.6. This data is for 60 nm titanium on silicon annealed at 650 °C.

The data is fit using equation 4.1 to fit the parabolic growth coefficient. In this case B is $0.001945 \text{ um}^2/\text{min}$. The FLOOPS simulation using this value is shown in Figure 4.7. Once again the reaction diffusion model does a good job of modeling the data.

4.2 Experiments in the RTA Growth of Titanium Disilicide

As can be seen from the previous sections there is quite a spread in silicide growth kinetics that depend on the type of annealing and the annealing ambient, as well as the film

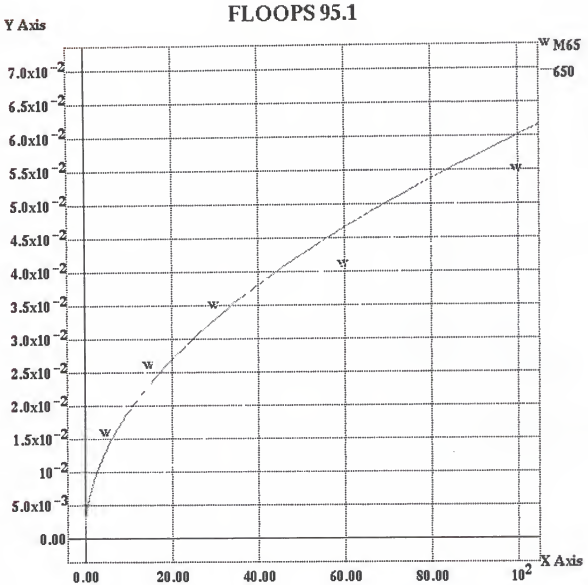


Figure 4-7: FLOOPS simulated silicide thickness versus anneal time.

deposition method and base pressure. All of the kinetics are diffusion limited and can be fit well using equation 4.1. Any two dimensional modeling of silicide growth will have to have accurate growth kinetics so that the silicide thickness versus time can be simulated. In support of the two dimensional experiments that will be discussed in chapter 5

some silicide thickness versus time experiments have been performed.

4.2.1 Overview of Experiment

The starting wafers were 10-20 Ω -cm p-type <100> silicon. The wafers were cleaned and then given a 30 second dip in 50:1 HF. The wafers were then immediately loaded into a Gryphon Sputterer. The sputterer was pumped down to approximately 5×10^{-8} Torr. Titanium films approximately 200 nm in thickness were then sputtered onto the wafers. The wafers were then annealed using a RTA for different times and temperatures.

The resulting film composition was then analyzed using Auger electron spectroscopy (AES) depth profiling with a Perkin-Elmer Model 660. The analytical conditions used were an electron beam current of 10 keV and 1.0 uA, the ion beam was 3keV and 2.8uA with a 2mm x 3mm raster area. The ion used to sputter the surface was Ar⁺. A stoichiometric sample of TiSi₂ was first analyzed to obtain the correct titanium and silicon sensitivity as well as sputter rate factor for TiSi₂.

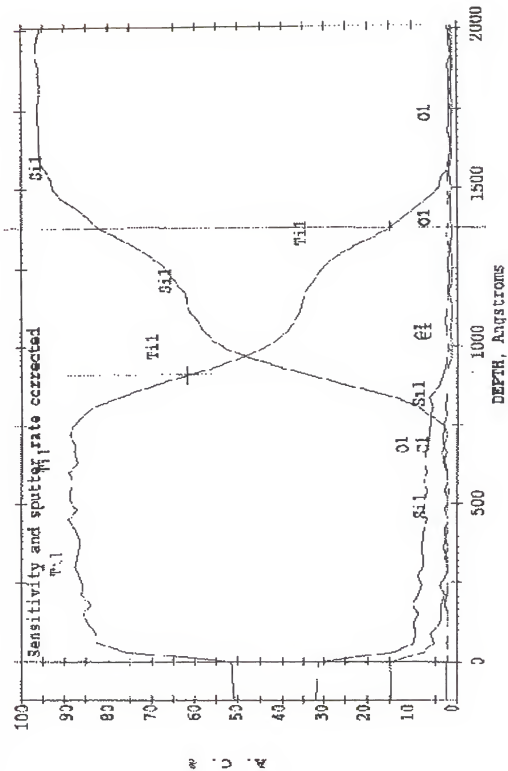


Figure 4-8: Sample AES plot showing thickness determination.

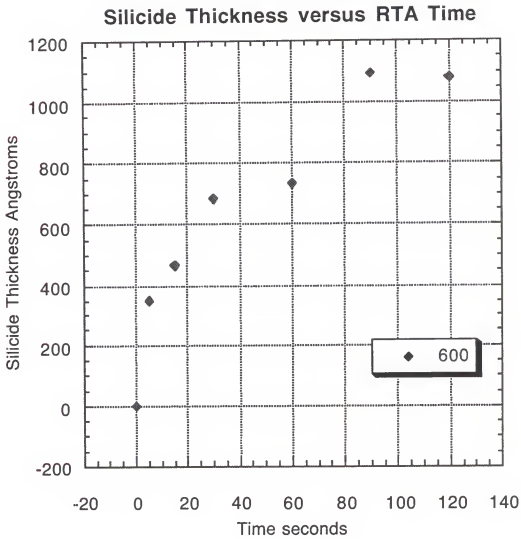


Figure 4-9: Silicide thickness versus RTA time at 600 °C.

4.2.2 Experimental Modeling

The samples composition versus depth was determined using AES. A sample AES plot is shown in Figure 4-8. The silicide thickness is determined as marked on the figure.

The 50% point for the titanium signal on each side of the interface is used to determine the interface location. It is difficult to determine the exact phase of the silicide present. The silicide at the silicon interface seems to be TiSi_2 and the composition is graded down to approximately TiSi . As can be seen in the AES spectra there is very little oxygen in the sample with the highest concentration at the $\text{TiSi}_x/\text{TiON}$ interface.

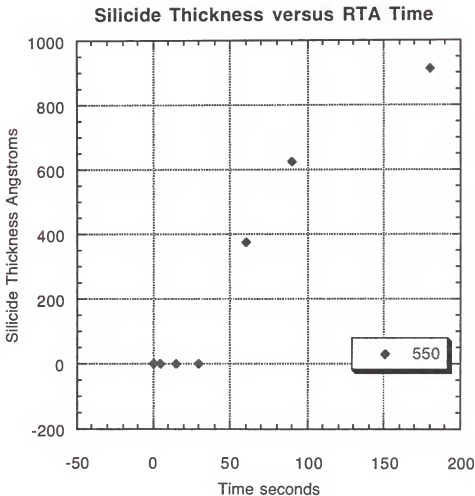


Figure 4-10: Silicide thickness versus RTA time at 550 °C.

The results for the 600 °C anneals are shown in Figure 4-9. The silicide thickness versus time once again displays diffusion limited growth. The results for the 550 °C anneals are shown in Figure 4-10. There is no noticeable silicide formation for anneals of 30 seconds or less. This is probably due both breaking down any native oxide on the

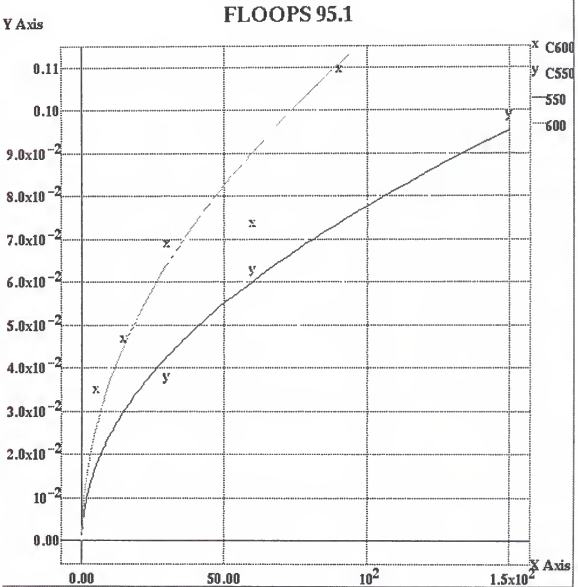


Figure 4-11: Comparison of RTA data to simulations.

silicon surface or nucleation of the silicide grains. The thickness versus time, if the curve is shifted so that the 30 seconds point is taken as the time zero, also exhibits diffusion limited growth.

The same procedure used in the previous sections is used to fit the data for the 600 and 550 °C anneals. Using Equation 4.3, the activation energy is found to be 1.0 eV and the pre-exponential term is $4.37\text{e}3 \text{ um}^2/\text{min}$. The simulations compared to data are shown in Figure 4-11 for both 550 and 600 °C anneals. The simulations fit the data well.

4.3 Summary

The previous four sections have discussed the modeling of four different experiments in titanium silicide growth kinetics. All of the experiments performed displayed diffusion limited growth behavior. The growth parameters of the silicide growth for the four experiments are plotted versus reciprocal temperature in degrees Kelvin in Figure 4-12. As can be seen there is quite a spread in the growth kinetics for each experiment. This is not very surprising especially considering the variety of titanium deposition techniques and conditions as well as the different annealing conditions used.

The samples in all four experiments were cleaned in a similar manner with an HF dip being the last step before

loading into the deposition chamber. Pico[24] and Hung[23] both used evaporation in order to deposit the titanium. The experiments done in this work as well as those carried out by

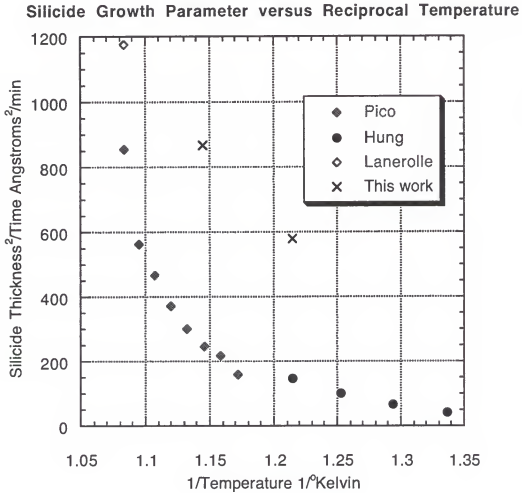


Figure 4-12: Silicide growth kinetics versus anneal temperature.

Lanorelle[39] used sputtering to deposit the films. Pico annealed his samples in a furnace under a vacuum as did Hung. Both of the rapid thermal annealed experiments were done in an nitrogen ambient. Rapid thermal annealed samples

will ramp up to the anneal temperature much faster than furnace annealed samples. The growth of TiN due to the nitrogen ambient will help cap the film from any oxygen in the annealing ambient. Overall the RTA results seem to have lower oxygen contamination which is probably why they are faster than the furnace annealed samples. Deposition techniques and parameters, especially the base pressure, will also be very important.

All of the silicide thickness data can be fit by the general reaction diffusion model from chapter 2. Equation 4.1 can be used to fit all of the data presented in this chapter. There does not seem to be a global set of growth parameters that can fit all of the data. Any use of this simulator for vastly different experimental conditions will need tuning of the parabolic growth parameter for the experimental conditions used. The main growth conditions that need to be kept track of are titanium deposition base pressure, silicon surface cleanliness, annealing ambient and equipment.

CHAPTER 5

TWO-DIMENSIONAL SILICIDE GROWTH EXPERIMENTS AND SIMULATIONS

The results of chapter 4 indicate that the general reactive diffusive model does a good job of simulating silicide thickness versus time data. The next step is to simulate two-dimensional structures, for example, a salicide process. Simulating two-dimensional shapes, as described in chapters 2 and 3, involves first solving for the diffusion and reaction of the diffusing species followed by accounting for the volume changes due to the reaction.

5.1 Two-Dimensional Salicide Simulations

The process steps of a typical salicide growth are discussed in section 1.2. The first anneal step is a less than 700 °C RTA in nitrogen. In order to simulate these two-dimensional structures both the formation of TiSi_2 and TiN must be solved for. The volume changes that occur due to the material growth must be taken into account as well as solving for the deformation of any surrounding materials.

The viscoelastic model of section 2.1.2.3 is used to model the deformation during silicide growth. There are a

number of coefficients needed to use this model. The values for Young's modulus and Poisson's ratio were taken from literature. The polysilicon values were taken to be less than the values for silicon and oxide so it would be the softest material in the system. When polysilicon is used in poly buffered LOCOS it helps absorb the stress from the nitride film so it seems reasonable to use soft values for the Young's modulus. The Young's modulus of TiN is calculated assuming a Poisson's ratio of 0.3 along with the measured shear modulus from Elana[40]. The coefficients for the viscoelastic model are shown in Table 5-1 for all of the materials involved in the salicide process. Some variation of these parameters should be expected as a function material deposition or growth conditions. All of the materials are treated as nearly elastic by using a high (1e17) viscosity.

Table 5-1: Mechanical parameters used to simulate silicide growth.

Material	Young's Modulus	Poisson's Ratio	Reference
TiSi ₂	1.42e12	0.27	Jongste[34]
Titanium	1.04e12	0.34	Pilkey[41]
Oxide	6.6e11	0.17	Ma[42]
Polysilicon	5e11	0.3	_____
TiN	2.78e12	0.3(assumed)	Elena[40]

The starting structure for the silicide simulations is generated using the rate based etching and deposit simulation capabilities of FLOOPS. The gate width is 0.35 μm and the gate oxide thickness is 10 nm. After patterning the gate the sidewall spacer is formed by isotropic SiO_2 deposition followed by anisotropic etching of the oxide. Next 40 nm of titanium is deposited. The structure before the first RTA is shown in Figure 5-1. The first anneal is for 30 seconds at 650 $^{\circ}\text{C}$. This anneal forms 42 nm of TiSi_2 . The simulation at this stage is shown in Figure 5-2. Comparison of this simulation to the thinning of the silicide at the spacer edge seen in Figures 1-3a and the poly smile seen in Figure 1-3b shows that the simulation shows neither of these effects. The simulated silicide sinks evenly into the polysilicon. The silicide also deforms the spacer at the silicide/spacer triple point. The undercut of the silicide under the spacer is also not seen experimentally. The areas where the simulation does not match the data are the areas of highest stresses. As mentioned in chapter 2 mechanical stress influences the growth of SiO_2 . It is possible that stress is influencing the growth of TiSi_2 . This leads to the experiment described in the next section.

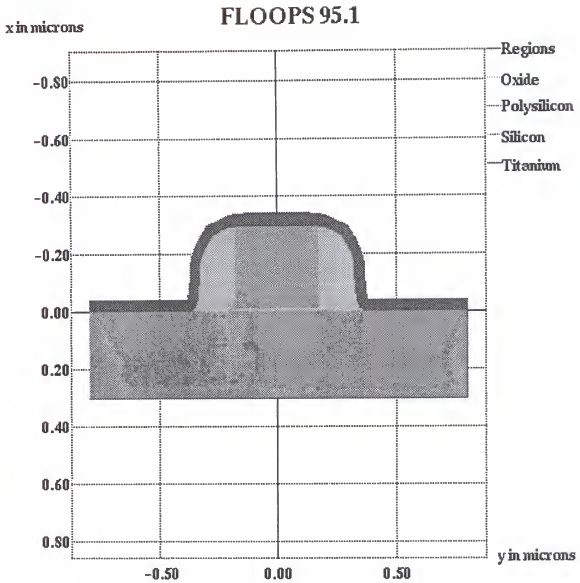


Figure 5-1: Simulated salicide structure before silicide formation.

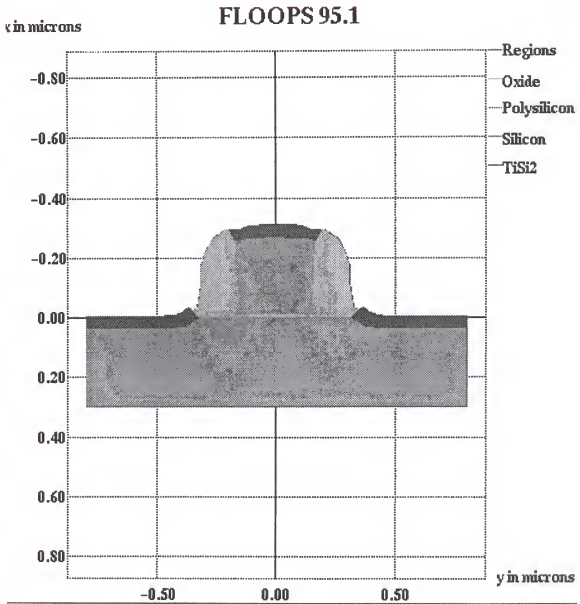


Figure 5-2: FLOOPS salicide simulation after silicide formation and strip of TiN and unreacted titanium.

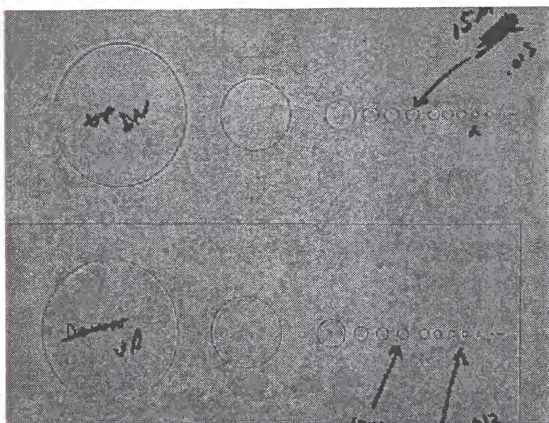


Figure 5-3: Photograph of cylinders and holes of various radius etched in silicon.

5.2 Two-Dimensional Experiments

In order to investigate the effect of stress on silicide growth, growth on curved surfaces was studied. Due to the volume change in silicide growth the stress increases for decreasing radius. The mask pattern used to induce stress into the growing silicide film is shown in Figure 5-3. It consists of cylinders and holes of various radii as well as lines or trenches. These structures were processed in two different experiments. The main differences between the

experiments were the silicon etch recipe and the deposited titanium thickness.

5.2.1 Experimental Design

P-type boron doped ($10\text{--}20\ \Omega\text{ cm}$), $\langle 100 \rangle$ oriented wafers were used in this study. The pattern shown in Figure 5-3 was patterned using standard photolithography techniques. The photoreresist is used as a mask for the silicon etch. As mentioned earlier there were two different sets of experiments sets A and B. The differences were in the silicon etch technique, etch depth, and deposited titanium thickness. Set A had a silicon etch depth of $0.5\ \mu\text{m}$. The etch was performed using a drytek reactive ion etcher. Set B had a silicon etch depth of $1.0\ \mu\text{m}$. The etch was performed using a CF_4 and O_2 chemistry in a Bransen plasma etcher. Both sets had titanium depositions in a Gryphon sputterer. The base pressure was approximately $5\text{e-}8$ Torr. Set A had $100\ \text{nm}$ of titanium deposited while set B had $200\ \text{nm}$ deposited. Set B was deposited at the same time as the wafers used in the growth kinetics experiments in chapter 4. Cross sectional Scanning Electron Microscopy (SEM) photographs of a set B wafer at this stage of the experiment is shown in Figure 5-4. Rapid thermal annealing (RTA) is used to form the silicide. The anneals were performed at $650\ ^\circ\text{C}$ for various times. The set B samples had RTA anneals of 30 and 60 seconds, samples S2 and S3 respectively. A sample from set B, sample P2, had

a 15 second anneal in the same RTA as the samples from chapter 4. The set A samples had a 30 second anneal. All the anneals were performed in a nitrogen ambient. The samples were analyzed using cross sectional SEM, AES, and top view and cross sectional Atomic Force Microscopy (AFM). The AFM was used in topographic mode.

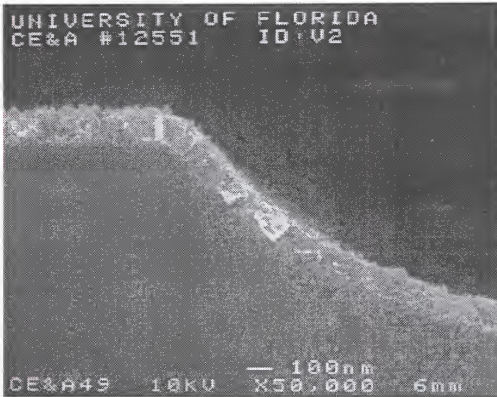


Figure 5-4: Cross sectional SEM of wafer from group B after titanium deposition.

5.2.2 Experimental Results

The first set of samples (set A) were initially analyzed using top view AFM. Both cylinders and holes of a few different radii were analyzed. Figure 5-5 shows the AFM plot

of a 7.5 μm diameter cylinder structure. The most interesting feature of the plot is the raised lip around the outer surface of the structure. This raised area was present on both cylinders and holes for different radius. This is interesting because this top corner is an area of the high compressive stress in the growing silicide film. The compressive stress arises because as new silicide is formed at the TiSi_2 /titanium interface it has to push the old silicide into a smaller volume area as the silicide sinks into the silicon.

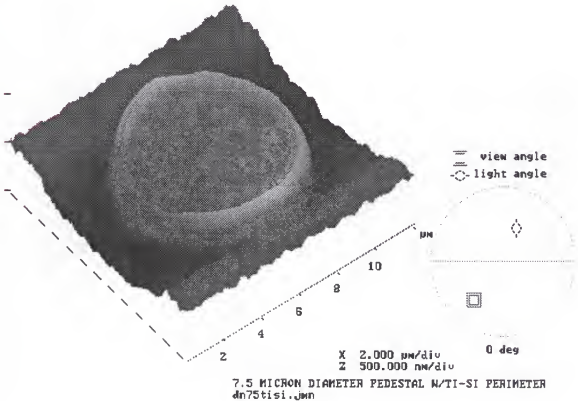


Figure 5-5: AFM plot showing the topography of a 7.5 μm diameter cylinder after TiSi_2 formation.

This interesting discovery led to investigation of the top corner of the lines in the pattern in Figure 5-3. This area of both (A and B) sets of samples was analyzed using cross sectional SEM. Figure 5-6 shows the SEM of a set A sample (C1) annealed for 30 seconds at 650 °C in an RTA. This sample was also analyzed using Auger Electron Spectroscopy (AES) on a planar surface on the wafer in the same manner as the samples of chapter 4. The titanium silicide thickness was measured to be 121 nm. It is evident from the SEM that there has been uneven silicon consumption near the top corner. This trend is evident in all the samples from both sets A and B. Figure 5-7 shows the SEM photograph of the S3 sample which also shows the same reduced silicon consumption at the high stress corner. Further SEM cross sections will be shown with the simulation results in the next section. AES analysis was also performed on the S3 and S2 samples. The P2 sample thickness was estimated from the growth kinetics found in chapter 4. This is because the sample was annealed in the same RTA as those samples and received the same deposition. The other samples were annealed in a different RTA. AES plots from samples S2 and S3 indicate that no TiN layer was formed. It is possible that there was a problem with the nitrogen ambient for those anneals. It did not seem to affect growth kinetics as the growth coefficient is higher for these samples than the growth coefficient found in chapter 4. Table 5-2 shows the RTA time and silicide

thickness and parabolic growth coefficient (B) for each sample. These parabolic growth coefficients will be used for simulation of the results of this section. Unfortunately silicide thickness grown on the side of the cylinders and holes versus the radius of curvature could not be extracted at this time. It is extremely difficult to see the difference between TiSi_2 , titanium and TiN in the SEM.

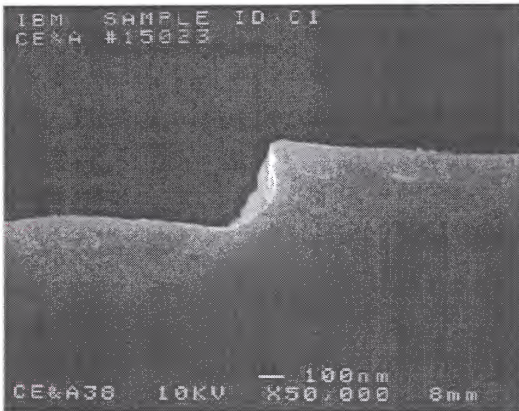


Figure 5-6: Cross sectional SEM photograph of sample C1 after 650 °C 30 second RTA.



Figure 5-7: Cross sectional SEM of sample S3 after TiSi_2 growth at 650 °C for 60 seconds.

Table 5-2: Silicide thickness and parabolic growth coefficients for the experimental samples.

Sample	Anneal Time (seconds)	Silicide Thickness (μm)	B ($\mu\text{m}^2/\text{min}$)
C4	30	0.121	0.0293
S2	30	0.1113	0.0248
S3	60	0.1576	0.0248
P2	15	0.0616	0.0152

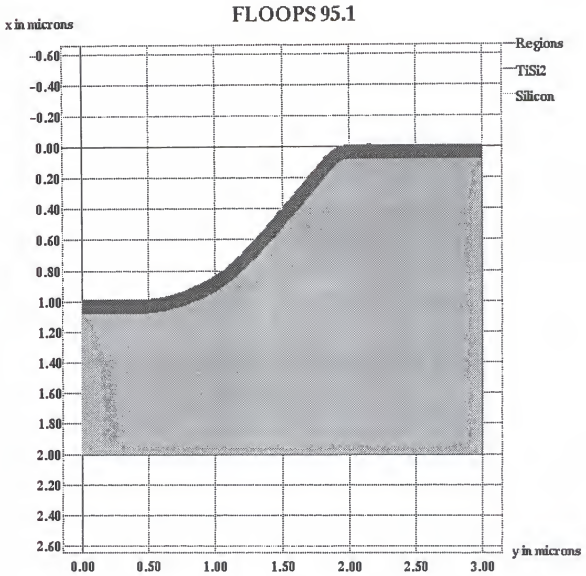


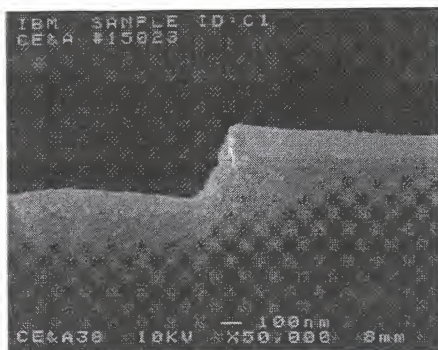
Figure 5-8: Viscoelastic simulation of silicide growth on a silicon trench showing even silicon consumption.

5.3 Stress Dependent Silicide Simulations

5.3.1 Simulation of Two-Dimensional Experiments

In order to simulate the experimental data seen in the previous section the coupled diffusion and flow problem must be solved. Figure 5-8 shows a linear viscoelastic simulation of a trench structure with no stress effects. Obviously this simulation does not accurately represent the trend seen in the previous section. The data from the previous section suggests that the mechanical stress caused by the growth around the trench corner is decreasing the diffusion of silicon through the silicide film. Unfortunately from the data in the previous section it is difficult to determine which flux is affected by the high stress region at the top trench corner. Any or all of the three fluxes discussed in chapter 2 could be affected by stress. Due to the fact that the growth of titanium silicide is diffusion limited it is hard to determine if the reaction of silicon with titanium is dependent on stress. It seems more likely that either the flux of silicon across the silicon/TiSi₂ interface or the diffusion of silicon through the silicide film would be stress dependent. The stress reduced diffusion of silicon flux is used here to model the data of stress dependent growth. Here the effective diffusivity is expressed as

a)



b)

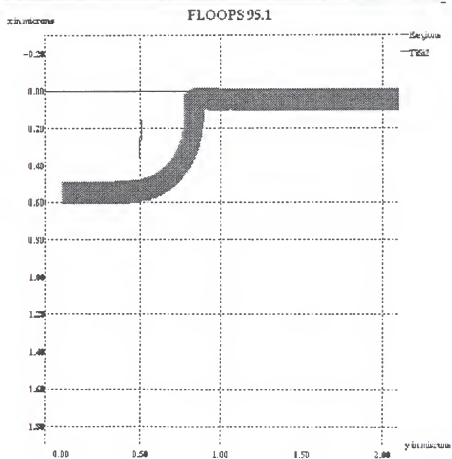


Figure 5-9: SEM photograph a) and simulated structure b) for sample C1.

$$D_{\text{eff}} = D_0 \exp\left(\frac{-PV_d}{kT}\right) \text{ for } P > 0 \quad (5.1)$$

where D_0 is the diffusivity from the growth coefficient, k is Boltzman's constant, T is the temperature in degrees Kelvin, P is the hydrostatic pressure (positive compression) and V_d is the activation volume for the stress reduced diffusion. This is the same expression that is used to model the stress dependent diffusion during oxide growth.

The parameters needed to simulate the experimental structures from the previous section are the parabolic growth coefficient (B), V_d from equation 5.1, and the mechanical parameters for the silicide growth materials, TiSi_2 and titanium. The mechanical parameters are taken from literature as is section 5.1 and are listed in Table 5-1. The parabolic growth coefficient are given in Table 5-2. The activation volume for the stress dependent diffusivity (V_d) is varied until the simulation matches the experimental structures. Using this approach the best fit for V_d is $2.5 \text{ } \text{\AA}^3$. The comparisons of the simulations to the experimental structures for each of the four samples described in the previous section are shown in Figure 5-9 through Figure 5-12. The unreacted titanium has been stripped off in the simulations while the experimental structures still have a top layer film containing TiN/TiO_2 and any unreacted titanium. The general trend of less silicon consumption from top corner is seen in all the simulations. This matches the

experiments well. The stresses which are calculated for in these simulations are very high, $> 1 \times 10^{10}$ dynes/cm², it is very likely that some form of plastic deformation has occurred in these samples. This was not simulated in these structures due lack of data that would support that plastic deformation is occurring.

5.3.2 Salicide Simulations

The simulations presented in the previous section imply that a stress dependent diffusivity can be used to explain the experimental results seen in section 5.2. As was mentioned earlier other stress effects on both the diffusion of silicon as well as the mechanical properties of the silicide films could be occurring. The next question to be answered is if a stress dependent diffusivity can produce better qualitative agreement for the simulation of salicide structures. The simulation without any stress dependent growth displays neither the poly smile nor the thinning or pinning of the silicide at the spacer edge. Unfortunately the simulation of salicide structures is much more complex because of the number of materials involved as well the number of reactions taking place. Titanium films are very reactive and can react with the annealing ambient to form TiN as well as reacting with the sidewall spacer. The exact kinetics of these reactions are not known.

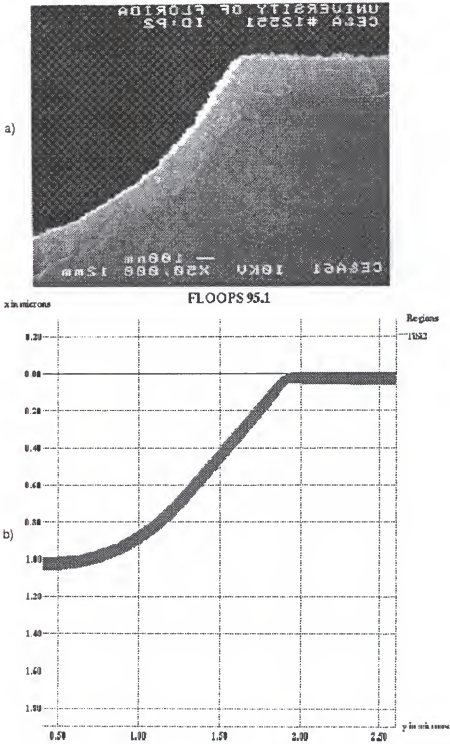
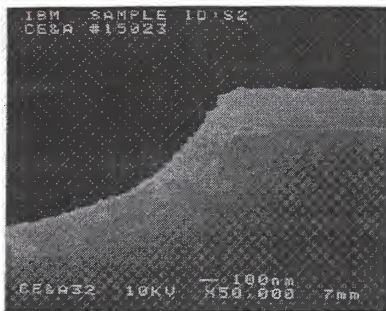


Figure 5-10: SEM photograph a) and simulated structure b) for sample P2.

a)



b)

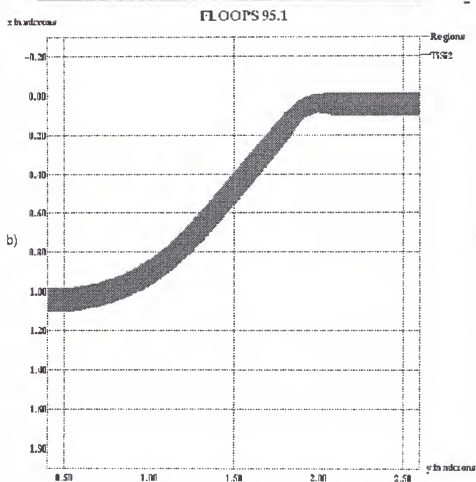


Figure 5-11: SEM photograph a) and simulated structure b) for sample S2.

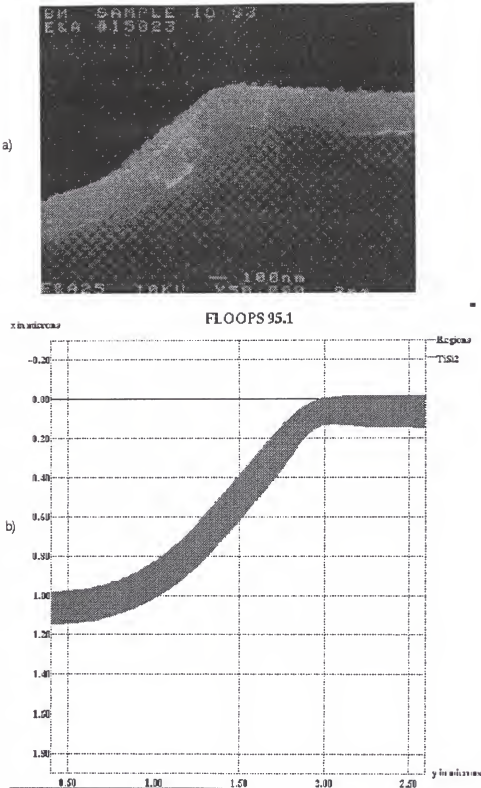


Figure 5-12: SEM photograph a) and simulated structure b) for sample S3.

Using the stress dependent diffusivity alone in the simulation from section 5.1 did not result in the correct results. The problem was that the consumption of the silicon from the triple points creates tensile stress in the silicide near the spacer. The next step was to pin the triple point by zeroing the mass transfer of silicon at the triple points. Using this in conjunction with a stiff (higher Young's modulus and viscosity) oxide created compressive stress in the silicide film and much more realistic silicide shapes in the silicide simulation. The simulation results for a 0.5 μm gate width are shown in Figure 5-13. The simulation shows both the polysilicon and the pinning of the silicide at the silicon/oxide spacer/ TiSi_2 triple point. The spacer needs to be stiff in these simulations so that the oxide doesn't flow in response to the volume change at the titanium/ TiSi_2 interface. The Young's modulus of the oxide was taken to be 6.6×10^{12} dynes/cm², which is high, for this simulation. The ratio of the Young's moduli for each material is important. Due to the high stress present in the system it is not unrealistic to expect some nonlinear or plastic flow in the materials. For this case it is possible that the plastic deformation would dominate and the important parameters would be which material flowed at a lower stress. The second assumption in this simulation is the reduction of the mass transfer at the oxide/silicide triple points which could also be due to stress at the corner, interaction with the spacer, or even stress in the polysilicon or silicon itself.

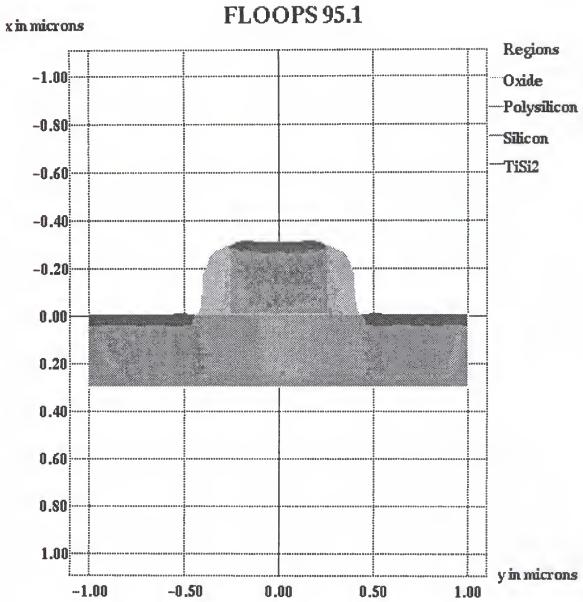


Figure 5-13: Salicide simulation of 0.5 μm gate width salicide structure.

5.4 Summary

Linear viscoelastic silicide simulations did not match the trends seen in literature for the silicide shapes. This led to the design and implementation of an experiment to determine if stress effects the growth kinetics of silicide formation. Titanium silicide films were grown on curved surfaces which resulted in large mechanical deformation of the growing silicide layers. This mechanical stress was found to reduce the growth in areas of high compressive pressure. Unfortunately the experiment did not yield a large amount of quantitative data but the qualitative trend was present. A stress dependent diffusivity was able to simulate the trends seen in the experimental data. There is not enough evidence to determine if other stress effects are occurring during the growth of TiSi_2 . Using the activation volume for the stress dependent diffusivity found by fitting the experimental structures along with a reduced transport of silicon at triple points produced more realistic looking simulations of silicide structures.

CHAPTER 6 THREE-DIMENSIONAL OXIDATION SIMULATIONS

This section will discuss the calibration of the oxide growth models with the ultimate goal being to test the three-dimensional code by simulating the three-dimensional oxidation data of Smeys[43,44]. As has been noted earlier in this work, the models of Senez et al.[45] are similar to the models used in this work. For whatever reason, be it different implementation or just calibration to different LOCOS data, his default coefficients have not worked well in simulating the two-dimensional structures of interest in this work. Due to this fact, his coefficients are not used in this work. Instead, the material models must be calibrated from data published in literature. First the stress dependent coefficients and viscosities are fit to the cylinder and hole oxidations by Kao[8]. Then the nitride coefficients will be fit using LOCOS shapes. These coefficients will then be compared to those of Senez[45]. Finally these coefficients will be used to simulate three-dimensional effects reported by Smeys[43]. Since this three-dimensional data is at 1000 °C, this is the only temperature at which the nitride coefficients will be fit. The same technique could be used to calibrate other temperatures of interest.

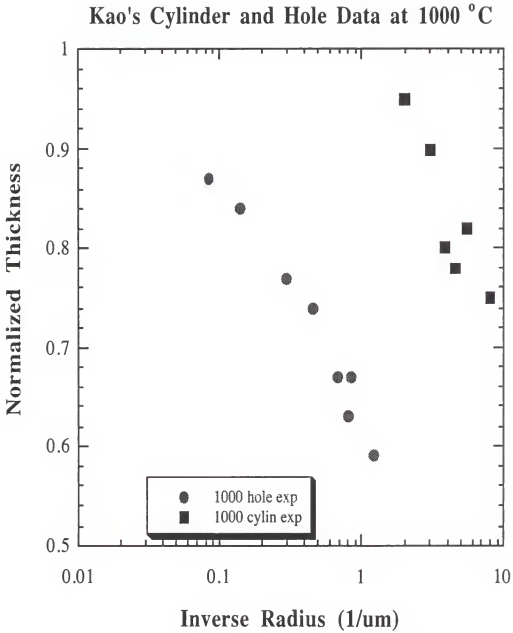


Figure 6-1: Normalized thickness versus final radius grown at 1000 °C.

6.1 Calibration of Oxide Models

6.1.1 Experimental Details and Results

The data used to calibrate the oxidation parameters is from the oxidation of cylinders and holes etched in silicon performed by Kao[8]. Cylinders and holes of varying radii were created by anisotropically etching silicon. These structures were then oxidized to grow approximately 5000 Å of SiO_2 at various temperatures. These structures were then coated with polysilicon and lapped down to the middle of the structures. Normalized oxide thickness grown on the different radii was then measured by SEM. The results of this experiment for 1000 °C in a wet ambient are shown in Figure 6-1. As can be seen the thickness grown on both convex (cylinders) and concave (holes) structures decreases with decreasing radius. It is also evident that the concave structures display a more severe retardation of oxide growth than convex structures.

The reasons for this decrease in thickness is due to stress effects on the diffusivity, reaction rates, and viscosity as discussed in chapter 2. Concave structures have compressive pressure and compressive stress normal to the Si/SiO_2 interface. Both of these stresses work to reduce the growth of SiO_2 . Convex structures produce a compressive stress normal to the Si/SiO_2 interface which reduces the reaction rate of oxide growth.

6.1.2 Calibration Procedure

The growth kinetics for the oxide are modeled using the Deal Grove method described in chapter 2. As described by Rafferty the default Deal Grove Parameters are off by as much as 50% from those in Kao's work. To take this into account he calculated B and B/A coefficients from Kao's data. These values are the ones used in this work. The other parameters for the simulations that can be taken from literature are the Young's modulus (Y_m) and Poisson's ratio (Pr) of the oxide. They are $Y_m=6.6e11$ and $Pr=0.17$ [41]. These are the same values used by Senez[45], which will allow direct comparison of the values calibrated in this work as well to those in their work. The oxide is treated as a viscoelastic material as described in chapter 2. The viscosity is dependent on shear stress, from chapter 2

$$\mu = \mu_0 \frac{\sigma_s / \sigma_c}{\sinh(\sigma_s / \sigma_c)} \quad 6.1$$

where σ_c is the critical stress for plastic flow. The critical stress is given by:

$$\sigma_c = \frac{kT}{V_c} \quad 6.2$$

where V_c is the activation volume for plastic flow, k is Boltzman's constant and T is the temperature in degrees Kelvin. The activation volume for plastic flow is one of the parameters used to calibrate the simulation to this data. The other parameters to calibrate are the activation volumes from equations 2.20 (V_r) and 2.21 (V_d) which account for the stress effects on reaction rate and diffusivity respectively.

This leaves us with four parameters to vary in order to fit Kao's data. They are μ_o , V_c , V_r and V_d . The procedure for calibration of the oxide parameters is similar to the method used by Rafferty[6] and Senez[45]. A value of V_d is picked and the large radii hole structures are simulated to find μ_o . Using these two parameters V_c is varied to fit the smaller radii hole data. Using these three known parameters, V_r is found by fitting the cylinder data. This is repeated until a good fit is obtained.

The fits achieved using this method is shown in Figures 6.2, 6.3 and 6.4 for 900, 1000, 1100 °C oxidations. The fits seem good and are as close to the data as any other sets published. The parameters found are shown in Table 6.1. The diffusivity activation volume was chosen to be 75 \AA^3 so that comparisons could be made to Senez's viscoelastic parameter set. The values found are similar to Senez's. Senez's value for V_r was 15 \AA^3 , which is close to the 10 \AA^3 found here especially considering the spread in the cylinder data. Senez's activation volumes are similar to the values found

here, they are 390, 425 and 1000 Å³ for 900, 1000 and 1100 °C respectively. The natural log of the low stress viscosity found in this work as well as those reported by Senez are plotted versus the reciprocal temperature in Figure 6-5. The values fit very well with the arhenous plot and the activation energy is -2.65 eV.

Table 6-1: Calibrated oxide parameters.

Temperature	V_d	V_r	μ_o	V_c
900	75	10	1.5e15	300
1000	75	10	2.0e14	450
1100	75	10	3.3e13	1100

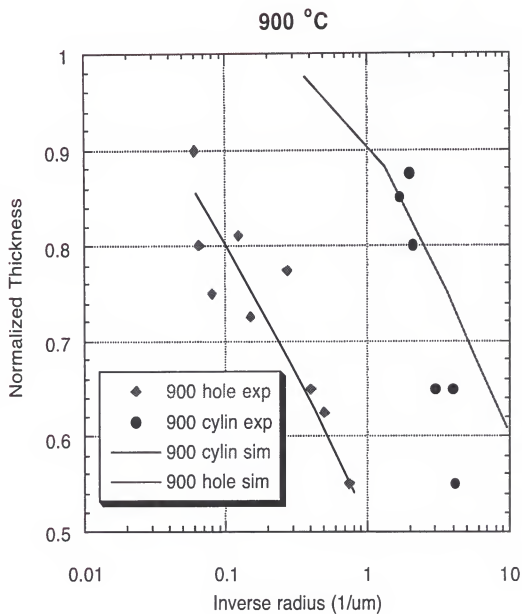


Figure 6-2: Comparison of simulation to experiment for 900 °C data.

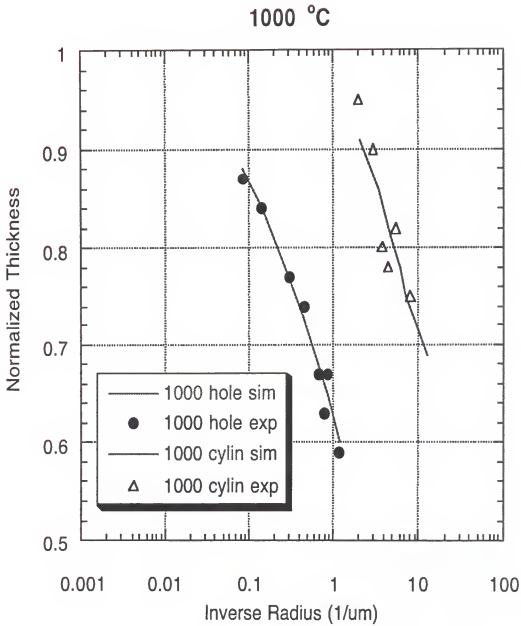


Figure 6-3: Comparison to Kao's experimental data at 1000 °C.

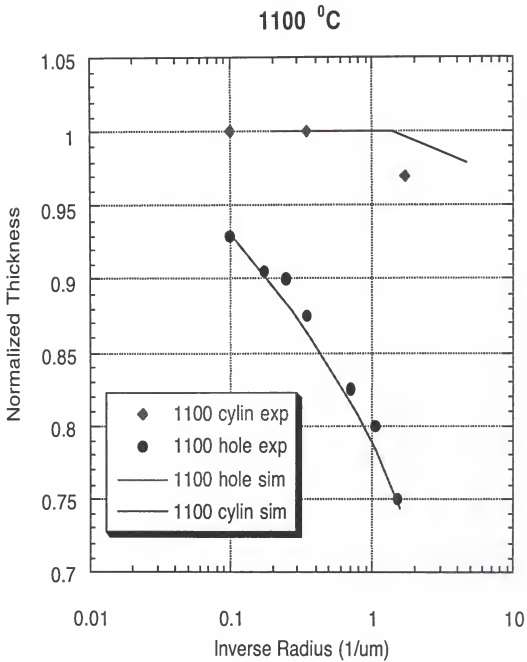


Figure 6-4: Comparison to Kao's data at 1100 °C.

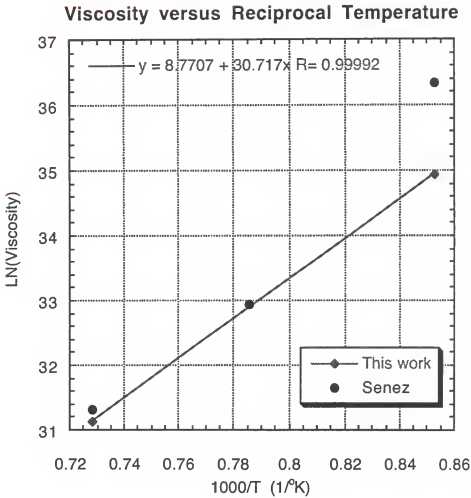


Figure 6-5: Natural log of viscosity versus reciprocal temperature.

6.2 Calibration of Nitride Models

Once stress dependent parameters have been found for the oxide models, LOCOS structures can be simulated in order to determine the parameters to use for the nitride material models. The nitride is also treated as nonlinear

viscoelastic material with stress dependent viscosity. The Young's modulus and Poisson's ratio are taken from literature[46]. They are $Y_m=3.89e12$ dynes/cm² and $Pr=0.3$. The value for the low stress viscosity μ_0 from fitting LOCOS shapes for thick nitride films while the activation volume for plastic flow (V_c) is deduced from thinner nitride films which experience more deformation and therefore more plastic flow, than thick films do.

The data used to calibrate the nitride viscosities is from Kenkare[2]. In this work LOCOS structures are grown at 1000 °C for 80 minutes. The structures have 15 nm padox thickness and nitride thicknesses of either 140 nm or 200 nm. The final oxide thickness is 500 nm. Various nitride widths were used ranging from greater than 2.0 μm to less than 0.4 μm . The 200 nm thick nitride case use widths of 0.4, 0.6 and greater than 5 μm . Transmission electron micrographs for each these structures are reported. For the case of the 140 nm thick nitride, bird's beak height versus nitride width are reported. The definition of bird's beak height is shown in Figure 6-6. The comparison of simulated and experimental bird's beak height versus nitride width is shown in Figure 6-7. The fits to the 200 nm cases are shown in Figure 6-8. The nitride parameters used to fit this data was μ_0 equal to $7e14$ poises and V_c equal to 100 \AA^3 . These values are significantly less than those reported by Senez, who reported a low stress viscosity of $5e15$ and a V_c of 170 \AA^3 .



Figure 6-6: Simulated LOCOS shape showing the definition of the bird's beak height (BBH).

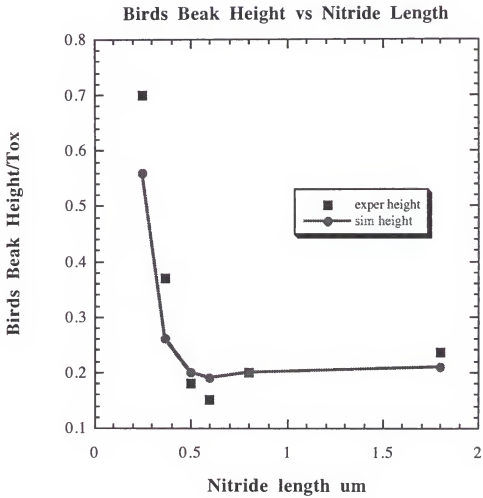


Figure 6-7: Comparison of simulation to experiment of the bird's beak height versus the nitride width.

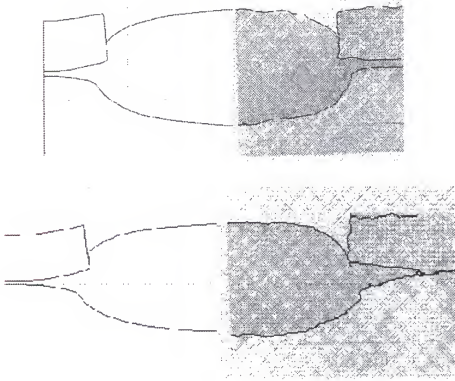


Figure 6-8: Simulated (left) and TEM micrographs of 0.6 μm wide nitride line and $>5.0 \mu\text{m}$ wide line.

6.3 Three-Dimensional Simulations

Smeys[43,44] designed and performed an experiment on three-dimensional effects in the LOCOS process. The pad oxide thickness in these structures was 10 nm while the nitride thickness was 150 nm. After patterning the nitride,

430 nm of field oxide was grown at 1000 °C in pyrogenic steam. The oxidation time was 70 minutes. The nitride was stripped, and the pad oxide was given a timed etch to remove 10 nm of oxide. Top view scanning electron microscopy (SEM) photographs were taken to measure the bird's beak length versus the width of the nitride lines. An example top view SEM photographs for nitride widths of 0.45 and 0.7 μm are shown in Figure 6-9. Also marked on the pictures are the bird's beak length under the tip (Lbb2) and under the line (Lbb1).

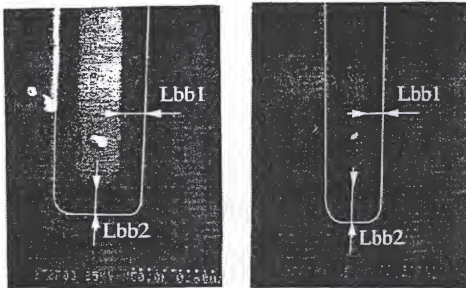


Figure 6-9: Top view SEM of LOCOS structures after nitride strip and pad oxide etch for 0.7 (left) and 0.45 (right) μm wide lines[44].

The nitride and oxide parameters fit from the two-dimensional data in the last two sections are used to simulate the LOCOS finger structures from Smeys' work.

Nitride lines 1.5 μm in length and with widths varying between 1.5 and 0.4 μm were simulated. The field oxide opening was 1.5 μm along both edges. Reflecting boundary conditions were used so 1/4 of the structure was simulated. Figure 6-10 shows the simulated structures for 1.5 and 0.4 μm wide nitride lines. The nitride line is lifted higher for the narrow line which agrees with the data reported by Smeys.

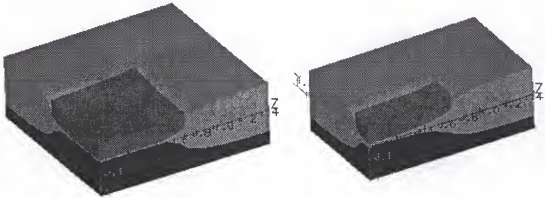


Figure 6-10: Three-dimensional LOCOS simulations of a 1.5 (left) and 0.4 (right) wide nitride lines.

In both two- and three-dimensional simulations the bird's beak length is overestimated with the nitride parameters found in the previous section. The bird's beak length is measured as the length from the edge of the nitride mask to the point where the oxide under the mask is 10 nm. Two-dimensional simulations were used in order to determine the oxide thickness under the nitride that resulted in a

bird's beak length of 0.19 μm . The thickness was 15.5 nm. This thickness is used to extract the bird's beak length versus nitride width along the long edge (Lbb2) and under the short edge (Lbb1). The results obtained using this technique compared to the experimental data are shown in Figure 6-11. The simulated results match the trend well for both the increase of Lbb2 with decreasing width and the decrease of Lbb1 with decreasing width.

There are several reasons why the nitride parameters determined in the previous section would over predict the bird's beak length. The main reason is probably just that the experiments were performed at different labs. In fact to get the thickness correct for Smeys' work the pressure had to be reduced to 0.9 (reducing the pressure scales both the linear and parabolic growth coefficients). There seems to be quite a lot of differences reported in the literature for structures with similar configurations. For example in a paper by Lee [47] there are LOCOS structures with 20 nm pad oxide and 140 nm nitride (compared to 15/140 used by Kenkare) that show less bird's beak height than do Kenkare's data. The structures were both grown at 1000 $^{\circ}\text{C}$. In fact Lee's structures had thicker oxide grown 590 nm to 500 nm. The main focus of this work has been the development of the three-dimensional simulation capability. There is good agreement between two-dimensional and three-dimensional simulations. The three-dimensional effects of increased

bird's beak length under narrow nitride fingers is captured by the simulations.

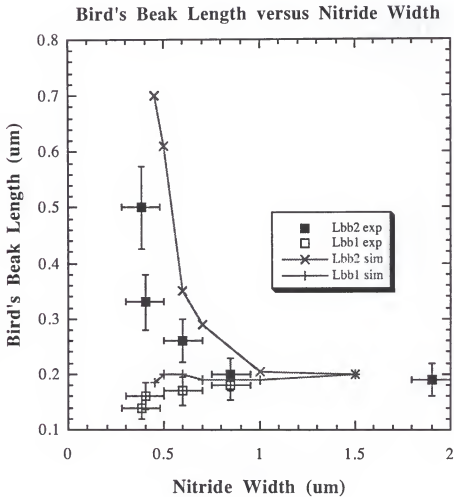


Figure 6-11: Comparison of simulation to the three-dimensional data of Smeys'.

6.4 Summary

In this chapter oxidation simulation has been used to simulate the cylinder and hole data from Kao[8], and two-

dimensional LOCOS structures from Kenkare[2]. The parameters found from simulating these structures were used to simulate the three-dimensional data from Smeys'[43]. The agreement between simulation and data is good. Better calibration of the nitride parameters is needed to take into account some of the spread of the data seen for LOCOS shapes from different experiments. Three-dimensional simulation captures the trend of increased lifting under the tip for narrow nitride lines.

CHAPTER 7

SUMMARY AND FUTURE WORK

This dissertation has described a multidimensional simulation program for semiconductor material growth modeling. The two material growth systems studied were silicon oxidation and titanium silicidation. Chapter 2 described the models used for the material growth simulation. The model consists of two main parts. First solve for the diffusion and reaction of the reactant and second account for the volume changes that occur due to the growth. A Deal Grove like reaction and diffusion model is used to solve for the diffusion and reaction of the reactant. The model consists of three fluxes. The flux of reactant from the reactant source, the diffusion of reactant through the growing film and the reaction flux. A viscoelastic model is used to solve for the material deformation that occurs due to the material growth. A viscoelastic model makes sense for a general growth code that needs to solve for material responses of a wide range of temperatures, strain rates, and material types. The stress from the volume changes can affect the diffusion and material parameters.

Chapter 3 describes how the models were implemented in the process simulator FLOOPS. The finite element method is

used to discretize both the diffusion and flow problems. Newton's method is used to solve for the nonlinearity caused by the stress dependent growth terms. Object oriented techniques were used in the development of this code because of the similarities between the material growth systems as well as the finite element numerics used for the different physical models. The object oriented nature of the code allowed code sharing between the different growth models and sped the development of new models. The addition of new material growth models like cobalt silicide growth or nitride oxidation during silicon oxidation is one area where future work would be possible. The numerics described in this section could also be a subject of future work. It is possible that some sort of line search technique used to find the best update at each Newton iteration would improve the convergence of the nonlinear iteration. Adaptive gridding on the nonlinear error could also improve convergence problems caused in three dimensional simulations where low quality grids can adversely affect the convergence. The recent results presented by Wang[48] which show improved grid quality while grid adaptation is taking place look promising. Adaptive gridding could also be performed on the error in the stress computation. The main challenge here would be to find an appropriate error indicator for the stress terms.

Chapter 4 described one dimensional simulation and experiments in TiSi_2 growth. Good fits were found for three different sets of published data in addition to the RTA

growth of TiSi_2 , experiment performed as part of this work. All of the growth data investigated displayed parabolic thickness versus time behavior indicating diffusion limited growth. The reaction diffusion model described in chapter 2 was used with a large reaction rate (large enough not to influence the growth). The only fitting parameter used in these simulations is B, the parabolic growth coefficient. There is quite a lot of spread in the tuned growth coefficients indicating that future use of these models will need local calibration of the parabolic growth coefficient. The main factors that seem to influence the growth are the titanium deposition conditions, surface cleaning, and annealing ambient and type. This work has just scratched the surface of tuning of this growth model. A more complicated model that solved for TiSi_2 and TiSi precursor is possible for one dimensional simulation[49]. This might be difficult to implement in two- and three-dimensions were the moving grid code could have problems. Better TiN growth coefficients are also necessary. Quantifying the effect of oxygen in the films and substrate doping on the growth rate would be interesting.

Chapter 5 first used the one dimensional growth rates from chapter 4 to simulate silicide structures. Neither the poly smile or the pinning of the silicide at the spacer edge is seen in linear viscoelastic simulation. Next an experiment on silicide growth around curved surfaces is discussed. The results indicate that high compressive

pressure is reducing the consumption of silicon. The stress is caused by the growth of the silicide at the top corner of a trench etched in silicon. A stress dependent diffusivity is used to qualitatively model the results seen for a samples annealed at 650 °C in an RTA for a few different times. Unfortunately the more quantitative data of stress versus radius of curvature for cylinder and hole patterns etched in the silicon could not be obtained. It is possible that with Transmission Electron Microscopy (TEM) the thickness of silicide formed on the cylinder sidewalls could be seen. Using the stress dependent diffusivity found from the trench results along with a reduced silicon transport at the spacer edge more realistic looking silicide simulations were obtained. There is a lot of experimental work that could be done to improve these simulations. The mechanical parameters for all the silicide materials should be obtained, especially their response under high stress conditions. Additional data on stress effects on silicide growth would help determine if any of the other fluxes are dependent on mechanical stress.

The final chapter of this work described the three-dimensional growth of silicon oxidation. The oxide stress dependent parameters were fit to Kao's cylinder and hole data[8]. The results are similar to those found by other researchers. The nitride viscosity and activation volume for plastic flow were tuned by simulating LOCOS shapes from Kenkare[2]. The parameters are lower than those extracted by Senez[45]. This is probably due to the difference in LOCOS

shapes each model was tuned to. Using these results the three dimensional data from Smeys[43] was simulated. The bird's beak length is overestimated in both two and three dimensional simulations. A higher nitride viscosity would decrease the results. When two-dimensional simulations are used to define the oxide thickness that matches the reported two-dimensional results, good agreement is found between simulation and experimental three dimensional results. Future work in this area includes tuning the nitride parameters over a wider range of temperatures. Experimental and simulation investigations of the oxidation of trench corners would be interesting. Also, investigation of the stress in silicon arising from isolation structures is becoming more important as device dimensions shrink and the device isolation structures are placed closer to active devices.

REFERENCES

- 1 T. Mizuno, S. Sawada, S. Maeda, and S. Shinozaki, "Oxidation Rate Reduction in Submicrometer LOCOS Process", *IEEE Trans. on Electron Devices*, vol. ED-34, p. 2255, 1987.
- 2 P. U. Kendare, J. R. Pfiester, J. D. Hayden, R. Subrahmanyam, R. I. Hedge and V. Kaushik, "Sensitivity of field isolation profiles to active pattern," *IEDM Tech. Dig.*, p. 479, 1993.
- 3 K. Maex, "Materials aspects of silicides for advanced technologies," *Appl. Surf. Sci.*, vol. 53, p. 328, 1991.
- 4 K. Maex and L Van den Hove, "The effect of silicides on the induction and removal of defects in silicon," *Mater. Sci. Engin.*, B4, p. 321, 1989.
- 5 H.C. Liu and S.P. Murarka, "Elastic and viscoelastic analysis of stress in thin films", *J. Appl. Phys.* vol.72, num. 8, p. 3458, 1992.
- 6 C. S. Rafferty, "Stress effects in silicon oxidation-simulation and experiments" Ph.D Dissertation, Stanford University, 1989.
- 7 B.E. Deal and A.S. Grove, "General relationship for the thermal oxidation of silicon," *J. Appl. Phys.*, vol. 36(12), p. 3370, 1965.
- 8 D. B. Kao, "Two-dimensional oxidation effects in silicon - experiments and theory," Ph.D Dissertation, Stanford University, 1986.
- 9 D. B. Kao, J.P. McVittie, William D. Nix and K.C. Saraswat, "Two dimensional silicon oxidation experiments and theory," *IEDM Tech. Digest*, p. 388, 1985.
- 10 M. E. Law, C. S. Rafferty and R. Dutton, *SUPREM4 Users Manual*, Stanford University, 1990.
- 11 P. Sutardja and W. G. Oldman, "Modeling of stress effects in silicon oxidation," *IEEE Trans. Electron Devices*, vol ED36, p. 2415, Nov. 1989.

- 12 D. Chin, S.Y. Oh, S.M. Hu, R.W. Dutton, and J.L. Mott, "A general solution method for two dimensional nonplanar oxidation," *IEEE Trans. Electron Devices*, vol. ED-30, p. 744, 1983.
- 13 H. Matsumoto and M. Fukuma, "Numerical modeling of nonuniform Si thermal oxidation", *IEEE Trans. Electron Devices*, vol. ED-32, p. 132 1985.
- 14 A. Poncet, "Finite-Element Simulation of Local Oxidation of Silicon," *IEEE Trans. Computer-Aided Design*, vol. CAD-4, p. 41, 1985.
- 15 H. Umimoto, S. Odanaka, I Nakao, and H. Esaki, "Numerical modeling of nonplanar oxidation coupled with stress effects," *IEEE Trans. on Computer-Aided Design*, vol. 8, p. 599, 1989.
- 16 H. Umimoto, S. Odanaka, "Three-Dimensional numerical simulation of local oxidation of silicon," *IEEE Trans. on Computer-Aided Design*, vol. 38, p. 505, 1991.
- 17 P.B. Griffin and C.S. Rafferty, "A viscous nitride model for nitride/oxide isolation structures," *IEDM Tech. Digest*, p. 741, 1990.
- 18 J.P. Peng, D. Chidambarrao and G.R. Srinivasan, "Novel: a non-linear viscoelastic model for thermal oxidation of silicon", *COMPEL*, vol.10, p. 341, 1991.
- 19 V. Senez, D. Collard and B. Baccus, "Quantitative 2D Stress Dependent Oxidation wiith ViscoElastic Model," *SISDEP Tech. Digest*, vol. 5, p. 165, 1993.
- 20 P.M. Fahey, S.R. Mader, S.R. Stiffler, R.L. Mohler, J.D. Mis, and J.A. Slinkman, "Stress-induced dislocations in silicon integrated circuits," *IBM Journal of Research and Development*, vol.36, p.158,1992.
- 21 S.M. Hu, "Stress-related problems in siicon technology," *J. Appl. Phys.*, vol. 70, p. R53, 1991.
- 22 J. Nagel, M. Reiche, S. Hopfe and D. Katzer, "Stress-induced void formation in interlevel polysilicon films during Polybuffered Local Oxidation of Silicon," *J. Electrochemical Soc.*, vol. 140, p. 2356, 1993.

- 23 L. S. Hung, J. Gyulai, J.W. Mayer, S. S. Lau, and M-A. Nicolett, "Kinetics of TiSi_2 formation by thin Ti films on Si," *J. Appl. Phys.*, vol. 54, p. 5076, 1983.
- 24 C. A. Pico and M. G. Lagally, "Kinetics of titanium silicide formation on single-crystal Si: Experiment and modeling," *J. Appl. Phys.*, vol. 64, p. 4957, 1988.
- 25 G. G. Bentini, R. Nipoti, A. Armigliato, M. Berti, A.V. Grigo and C. Cohen, "Growth and structure of titanium silicide phases formed by thin Ti films on Si crystals," *J. Appl. Phys.*, vol. 57, p. 270, 1985.
- 26 W. Tsai, M. Delfino, M.E. Day and J. A. Fair, "Effect of electron cyclotron resonance H^+ , Ne^+ , Ar^+ , and Xe^+ plasma precleaning on titanium silicide formation," *IEEE Trans. Electron Devices*, vol.41, p.1396, 1994.
- 27 K. Maex, "Silicides for integrated circuits: TiSi_2 and CoSi_2 ," *Materials Science and Engineering*, vol. R11, p. 53, 1993.
- 28 J. S. Choi, Y. S. Hwang, S.H. Paek, J. E. Oh, T. U. Sim and J. G. Lee, "Effects of BF_3 implants on titanium silicide formation by rapid thermal annealing," *J. Appl. Phys.*, vol. 72, p. 297, 1992.
- 29 R. Beyers, D. Coulman and P. Merchant, "Titanium disilicide formation on heavily doped silicon substrates," *J. Appl. Phys.*, vol. 61, p. 5110, 1987.
- 30 Y. L. Corcoran, A. H. King, N. de Lanerolle and B. Kim, "Grain boundary diffusion and growth of titanium silicide layers on silicon," *J. of Electronic Materials*, vol. 19, p. 1171, 1990.
- 31 G. J. P. Krooshof, F. H. P. M. Habraken, W. F. van der Weg, L. Van den hove, K. Maex, and R. F. De Keersmaecker, "Study of the rapid thermal nitridation and silicidation of Ti using elastic recoil detection. 1. Ti on Si," *J. Appl. Phys.* vol. 63, p. 5104, 1988.
- 32 J. F. Jonste, F. E. Prins, G. C. A. M. Janssen and S. Radelaar, "Modeling the formation of TiSi_2 in a nitrogen ambient," *Appl. Surf. Science*, vol. 38, p. 57, 1989.
- 33 J. F. Jongste, G. C. A. M. Janssen and S. Radelaar, "Formation of titanium disilicide during rapid thermal

- annealing, observed by in-situ stress measurements," *Appl. Surf. Science*. vol. 53, p. 212, 1991.
- 34 J.F. Jongste, O. B. Loopstra, G. C. A. M. Janssen and S. Radelaar, "Elastic constants and thermal expansion coefficient of metastable C49 TiSi₂," *J. Appl. Phys.*, vol. 73, p. 2816, 1993.
- 35 S. C. Chen, H. Tamura, T. Hara, K. Kinoshita, K. Inoue, N. Endo and S. Nakamura, "Silicidation reaction and stress in Ti/Si," *Jpn. J. Appl. Phys.*, vol. 31, p. 2673, 1992.
- 36 V. Svilar, J. M. E. Harper, C. Cabral Jr., and L.A. Clevenger, "Stress Evolution during the formation and transformation of titanium silicide," *Materials Research Society Proceedings*, vol. 365, p. 167, 1995.
- 37 T. C. Chou, C. Y. Wong and K. N. Tu, "Lattice imaging of metastable TiSi₂," *J. Appl. Phys.*, vol. 62, p. 2275, 1987.
- 38 O. C. Zienkiewicz and R. L. Taylor, *The Finite Element Method*, Fourth Edition, Vol. 1, (McGraw-Hill Book Company, New York, 1989).
- 39 N. de Lanerolle, D. Hoffman, and D. Ma, "Titanium silicide growth by rapid thermal processing of Ti films deposited on lightly doped and heavily doped silicon substrates," *J. Vac. Sci. Tech.*, vol. B5, p. 1689, 1987.
- 40 M. Eleana, M. Bonelli, C. E. Bottani, G. Ghislotti, A. Miotello, P. Mutti and P.M. Ossi, "Elastic behavior of TiN thin films," *Thin Solid Films*, vol. 236, p.236, 1993.
- 41 Pilkey, Walter D., *Formulas for Stress, Strain and Structural Matrices*, (John Wiley & Sons, Inc., New York, 1994).
- 42 T.P. Ma, "Stress in SiO₂-ON-Si structures," in *Properties of Silicon*, EMIS Datareview No. 4. London: ISSPEC, p. 650, 1987.
- 43 P.I.L. Smeys, P. B. Griffin, K.C. Saraswat, "Geometry dependence of void formation in deep submicron poly-buffered LOCOS isolation structures: experimental evidence of a stress relaxation model," *Fifth ULSI Symposium*, Electrochemical Society Proceedings, vol. 95-5, p. 94, 1995.

- 44 H. Park, P. Smeys, Z.H. Sahul, K.C. Saraswat, R. W. Dutton, and H. Hwang, "Quasi-Three-Dimensional Modeling of Sub-Micron LOCOS Structures," *IEEE Trans. on Semiconductor Manufacturing*, vol. 8, p. 390, 1995.
- 45 V. Senez, D. Collard, P. Ferreira, and B. Baccus, "Two-dimensional simulation of local oxidation of silicon: calibrated viscoelastic flow analysis," *IEEE Trans. on Electron Devices*, vol. 43, p. 720, 1996.
- 46 E.A. Irene, "Residual stress in silicon nitride films," *J. Electron Mater.*, vol.5, p. 2323, 1976.
- 47 Jun-ha Lee, M.S. Soo and H. J. Hwang, " Three-dimensional oxidation simulation with elasto-plastic model," Fourth International Symposium on Process Physics and Modeling in Semiconductor Technology, Electrochemical Society, vol. 96-4, p.228, 1996.
- 48 Everett X. Wang, M.D. Giles, S. Yu. F. A. Leon, A. Hiroki, and S. Odanaka, "Recursive M-tree method for 3-d adaptive tetrahedral mesh refinement and its application to brillouin zone discretization," *SISPAD 96 Proceedings*, p. 67, 1996.
- 49 L. Boruki, R. Mann, G. Miles, J. Slinkman, and T. Sullivan, " A model for titanium silicide film growth," *IEDM Tech. Dig.*, p. 348, 1988.

BIOGRAPHICAL SKETCH

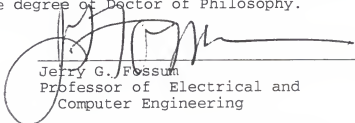
Stephen Cea was born on December 22, 1967, in New York, New York. He received his Bachelor of Science degree in electrical engineering in May, 1990 from the University of New Hampshire. He received his Masters of Science degree in December of 1993 from the University of Florida. Since then he has worked toward his Ph.D at the University of Florida. His research has focused on multidimensional models for semiconductor material growth processes.

I certify that I have read this study and that in my opinion it conforms to acceptable standards of scholarly presentation and is fully adequate, in scope and quality, as a dissertation for the degree of Doctor of Philosophy.



Mark E. Law, Chairman
Associate Professor of Electrical
and Computer Engineering

I certify that I have read this study and that in my opinion it conforms to acceptable standards of scholarly presentation and is fully adequate, in scope and quality, as a dissertation for the degree of Doctor of Philosophy.



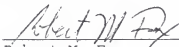
Jerry G. Fossum
Professor of Electrical and
Computer Engineering

I certify that I have read this study and that in my opinion it conforms to acceptable standards of scholarly presentation and is fully adequate, in scope and quality, as a dissertation for the degree of Doctor of Philosophy.



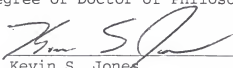
Sheng S. Li
Professor of Electrical and
Computer Engineering

I certify that I have read this study and that in my opinion it conforms to acceptable standards of scholarly presentation and is fully adequate, in scope and quality, as a dissertation for the degree of Doctor of Philosophy.



Robert M. Fox
Associate Professor of Electrical
and Computer Engineering

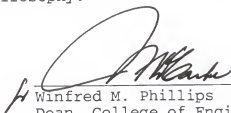
I certify that I have read this study and that in my opinion it conforms to acceptable standards of scholarly presentation and is fully adequate, in scope and quality, as a dissertation for the degree of Doctor of Philosophy.



Kevin S. Jones
Associate Professor of Materials
Science and Engineering

This dissertation was submitted to the Graduate Faculty College of Engineering and to the Graduate School and was accepted as partial fulfillment of the requirements for the degree of Doctor of Philosophy.

December, 1996

A handwritten signature in dark ink, appearing to read 'W. M. Phillips', is written over a horizontal line.

Winfred M. Phillips
Dean, College of Engineering

Karen A. Holbrook
Dean, Graduate School